INTERCOMPARISON OF METHODS FOR ESTIMATING LEAF ANGLE DISTRIBUTION WITH TERRESTRIAL LIDAR FOR BROADLEAF TREE SPECIES

CHRIS MUTUGI MURITHI
June 2023

SUPERVISORS:
Dr. Jan Pisek
Prof. Dr A. K. Skidmore

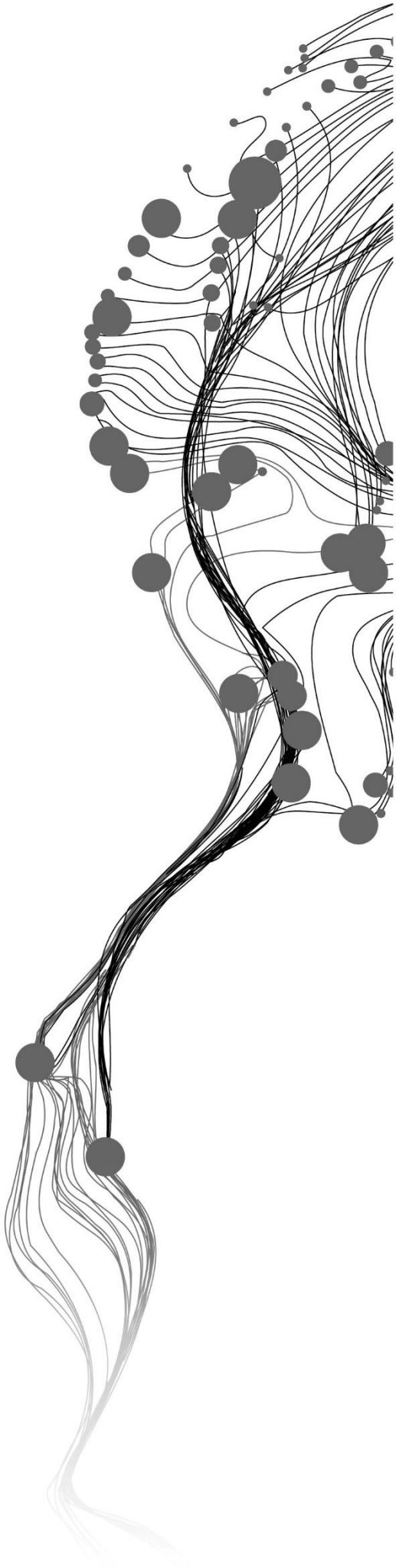

INTERCOMPARISON OF METHODS FOR ESTIMATING LEAF ANGLE DISTRIBUTION WITH TERRESTRIAL LIDAR FOR BROADLEAF TREE SPECIES

CHRIS MUTUGI MURITHI
Enschede, The Netherlands, June 2023

Thesis submitted to the Faculty of Geo-Information Science and Earth Observation of the University of Twente in partial fulfilment of the requirements for the degree of Master of Science in Geo-information Science and Earth Observation.
Specialisation: Geo-information science and Earth observation for environmental modelling and management for Urban-Rural Interactions

SUPERVISORS:
Dr. Jan Pisek
Prof. Dr. A.K. Skidmore

THESIS ASSESSMENT BOARD:
Dr. R. Darvishzadeh Varchehi (Chair)
Dr. Francesco Chianucci (External Examiner, Council for Agricultural Research and Agricultural Economy Analysis, Italy)
Drs. R.G. Nijmeijer (Procedural advisor)

ABSTRACT

Monitoring changes in biodiversity and understanding their impact on society is crucial for conservation efforts and ecosystem management. Essential Biodiversity Variables (EBVs) have been established as a standardised framework to comprehend and track biodiversity changes, supporting these efforts. One key EBV that provides valuable information on ecosystem structure and function is the Leaf Area Index (LAI), a critical biophysical parameter of vegetation. The estimation of LAI using indirect methods is highly dependent on the leaf angle distribution (LAD). However, accurately measuring LAD has been challenging, leading to the limited characterisation of this parameter. It is often simplified using predefined mathematical functions, overlooking its actual variation. In recent years, Terrestrial Laser Scanning (TLS) instruments have emerged as valuable tools for acquiring detailed measurements of canopy structure. Various methods have been proposed to extract LAD information from TLS data, but the intercomparison of these methods is yet to be reported.

This study addressed this gap by testing and comparing available TLS-based algorithms for estimating LAD using real tree data obtained from terrestrial Light Detection and Ranging (LiDAR) scans. The performance of these TLS-based algorithms was also evaluated against the established levelled digital photography (LDP) approach, and simulated LiDAR data from synthetic 3D tree models was used for further analysis. The inter-comparison results indicated that, while there were some notable variations, most TLS-based algorithms did not exhibit significant differences in their LAD estimates for real trees when compared to other algorithms. Among the TLS-based algorithms, the Bailey and Mahaffee (2017), Point Cloud Library (PCL), Vicari et al. (2019), and Zheng and Moskal (2012) algorithms demonstrated better performance than the Liu et al. (2019) and Stovall et al. (2021) algorithms, which performed poorly in their LAD estimation. Furthermore, the use of synthetic scans revealed that TLS algorithms showed better performance in estimating LADs that had more leaf area facing the scanner's direction. The study highlighted that the algorithms that used merged point clouds performed better than their single-scan counterparts. Overall, TLS offered a more comprehensive representation of the canopy structure, capturing the entire canopy height profile and overcoming the limitations of the LDP approach. Benchmark datasets, evaluation protocols and availability of algorithms shall promote fairness, reproducibility, and the advancement of LAD estimation techniques by enabling researchers to identify strengths, weaknesses, and further areas for improvement in their algorithms.

Keywords: 3D, Leaf angle distribution (LAD), Levelled digital photography (LDP), Light detection and ranging (LiDAR), Terrestrial laser scanning (TLS)

ACKNOWLEDGEMENTS

First, I would like to express my deepest gratitude and appreciation to the Almighty God for His unwavering guidance and sustenance throughout my academic journey. His presence and blessings have been a source of strength, inspiration, and reassurance during the challenges and triumphs encountered.

I am deeply grateful for the invaluable guidance and support from my first supervisor, Dr. Jan Pisek, during my research journey. His expert advice, constructive feedback, thought-provoking discussions, and constant encouragement have played a pivotal role in shaping the outcome of my thesis. Additionally, I extend my deep gratitude to my second supervisor, Prof. Dr. Andrew K. Skidmore, for providing insightful feedback and creative ideas that have greatly enhanced the quality of my work.

I would also like to thank Dr. R. Darvishzadeh Varchehi, the Chair of my thesis defence, for her constructive criticism and valuable guidance in refining my research. I am also grateful to Drs. Raymond Nijmeijer, the NRM and GEM course coordinator, for his guidance and facilitation of the GEM programme and thesis process.

Additionally, I want to express my appreciation to the GEM Joint Master program and the associated institutions, namely the University of Tartu and the University of Twente, for granting me the invaluable opportunity to be part of this exceptional program. Through this experience, I have had the privilege of connecting with individuals from diverse backgrounds across the globe, which has enriched my academic journey. I am genuinely grateful for the knowledge, support, and lifelong connections I have gained through this remarkable program.

Special thanks to researchers Atticus Stovall, Brian Bailey, Guang Zheng, Jing Liu, and Matheus Vicari for generously sharing their algorithms and providing valuable insights into their functionality for this study. I am also grateful to Andres Kuusk for his invaluable guidance in setting up the Point Cloud Library and to Daniel Schraik for his tremendous support with the Kumpula dataset.

Lastly, I want to express my heartfelt appreciation to my family for their unwavering love and support throughout this journey.

TABLE OF CONTENTS

ABSTRACT i
ACKNOWLEDGEMENTS ii
TABLE OF CONTENTS iii
LIST OF FIGURES iv
LIST OF TABLES v
ACRONYMS vi
1. INTRODUCTION 1
1.1. Background 1
1.2. Leaf Area Index 1
1.3. The G-Function 2
1.4. Research Gap and Scientific Contribution 3
1.5. Problem Statement 4
1.6. Research Objectives and Questions 4
2. STUDY AREA, DATA, AND ALGORITHMS 5
2.1. Study Areas 5
2.2. Algorithms and Data 6
3. METHODOLOGY 9
3.1. Data Pre-processing 9
3.2. Leaf-wood Separation 9
3.3. Estimation of Leaf Inclination Angles 10
3.4. Leaf Inclination Angle Distribution 10
3.5. Statistical Analysis 12
3.6. Generation of 3D Synthetic Trees 12
3.7. Performance Evaluation of LAD Estimation Methods 12
4. RESULTS 14
4.1. LAD Estimation of Real Trees with TLS and LDP 14
4.2. Statistical Analysis 20
4.3. Performance Evaluation of Algorithms with Synthetic Data 22
6. CONCLUSION AND RECOMMENDATIONS 38
6.1. Conclusion 38
6.2. Recommendations for Future Research 38
LIST OF REFERENCES 39

LIST OF FIGURES

Figure 1: Location map of the Royal Botanic Gardens at Kew 5
Figure 2: Location map of the Kumpula Botanic Garden 6
Figure 3: The overall study workflow 9
Figure 4: The six classical predefined mathematical functions by De Wit (1965). Credit: Liu et al., 2019 and Canopy — *SCOPE 1.8 Documentation*, respectively. 11
Figure 5: A sample of the synthetic scan metadata for one scanner position 13
Figure 6: (a) An image of *Pyrus communis 'Olga'* (b) Fitted beta distributions of leaf inclination angles for *Pyrus communis 'Olga'* for each TLS algorithm and the LDP approach. 15
Figure 7: (a) An image of *Quercus robur* (b) Fitted beta distributions of leaf inclination angles for *Quercus robur* for each TLS algorithm and the LDP approach 16
Figure 8: (a) An image of *Rhododendron cf branchycarpum* (b) Fitted beta distributions of LIAs for *Rhododendron cf branchycarpum* 16
Figure 9: (a) An image of *Fagus sylvatica* (b) Fitted beta distributions of LIAs for *Fagus sylvatica* 17
Figure 10: (a) An image of *Wollemia nobilis* (b) Fitted beta distributions of LIAs for the *Wollemia nobilis* 18
Figure 11: (a) An image of *Ginkgo biloba* (b) Fitted beta distributions of LIAs for *Ginkgo biloba* 18
Figure 12: (a) An image of *Ostrya japonica.* (b) Fitted beta distributions of LIAs for *Ostrya japonica.* 20
Figure 13: (a) An image of *Diospyros lotus.* (b) Fitted beta distributions of LIAs for *Diospyros lotus.* 20
Figure 14: (a) A 3D model of a synthetic tree with spherical LAD. (b) A leaf-only 3D model of the same synthetic tree. 22
Figure 15: Fitted beta distributions of LIAs for the simulated spherical LAD tree representation. 23
Figure 16: Comparative analysis results for the synthetic spherical TLS dataset at 5-degree intervals, with shaded regions indicating a statistically significant difference between the synthetic model and the LAD estimation method. 24
Figure 17: Fitted beta distributions of LIAs for the simulated uniform LAD tree representation. 25
Figure 18: Comparative analysis results for the synthetic uniform TLS dataset at 5-degree intervals, with shaded regions indicating a statistically significant difference between the synthetic model and the LAD estimation method. 26
Figure 19: Comparative analysis results for the synthetic erectophile TLS dataset at 5-degree intervals, with shaded regions indicating a statistically significant difference between the synthetic model and the LAD estimation method. 28
Figure 20: Fitted beta distributions of LIAs for the simulated erectophile LAD tree representation. 29
Figure 21: An image of a *Rhododendron cf branchycarpum* shrub tree showing an upright or vertical leaf orientation, characteristic of the plant's growth during more favourable summer conditions. Credit: Prof. Dr. A.K. Skidmore. 30

LIST OF TABLES

Table 1: A summary of the publications and their corresponding shorter naming used in this study for reference 7
Table 2: Statistical results of the LAD retrieval methods for the *Pyrus communis 'Olga'* (i.e., the average leaf inclination angle in degrees (ALIA), standard deviation (SD), two parameters (μ and ν), LAD type based on De Wit (1965) (Distribution) and the number of normals' replicates (NR)). 14
Table 3: Statistical results for the LAD retrieval methods for *Quercus robur* (i.e., the average leaf inclination angle in degrees (ALIA), standard deviation (SD), two parameters (μ and ν), LAD type based on De Wit (1965) (Distribution) and the number of leaf normal replicates (NR)). 15
Table 4: Statistical results for the LAD retrieval methods for *Rhododendron cf branchycarpum* (i.e., the average leaf inclination angle in degrees (ALIA), standard deviation (SD), two parameters (μ and ν), LAD type based on De Wit (1965) (Distribution) and the number of leaf normal replicates (NR)). 16
Table 5: Statistical results for the LAD retrieval methods for *Fagus sylvatica* (i.e., the average leaf inclination angle in degrees (ALIA), standard deviation (SD), two parameters (μ and ν), LAD type based on De Wit (1965) (Distribution) and the number of leaf normal replicates (NR)). 17
Table 6: Statistical results for the LAD retrieval methods for *Wollemia nobilis* (i.e., the average leaf inclination angle in degrees (ALIA), standard deviation (SD), two parameters (μ and ν), LAD type based on De Wit (1965) (Distribution) and the number of leaf normal replicates (NR)). 18
Table 7: Statistical results for the LAD retrieval methods for *Ginkgo biloba* (i.e., the average leaf inclination angle in degrees (ALIA), standard deviation (SD), two parameters (μ and ν), LAD type based on De Wit (1965) (Distribution) and the number of leaf normal replicates (NR)). 19
Table 8: Statistical results for the LAD retrieval methods for *Ostrya japonica* (i.e., the average leaf inclination angle in degrees (ALIA), standard deviation (SD), two parameters (μ and ν), LAD type based on De Wit (1965) (Distribution) and the number of leaf normal replicates (NR)). 19
Table 9: Statistical results for the LAD retrieval methods for *Diospyros lotus* (i.e., the average leaf inclination angle in degrees (ALIA), standard deviation (SD), two parameters (μ and ν), LAD type based on De Wit (1965) (Distribution) and the number of leaf normal replicates (NR)). 20
Table 10: Pairwise comparison of P-values from the Mann-Whitney U-test for the trees at the Kumpula Botanic Garden. Cells highlighted in light red indicate p-values < 0.05, while those in light green represent p-values > 0.05. 21
Table 11: Pairwise comparison of P-values from the Mann-Whitney U-test for the trees at the Royal Botanic Garden at Kew. Cells highlighted in light red indicate p-values < 0.05, while those in light green represent p-values > 0.05. 22
Table 12: Ranking of TLS algorithms based on their processing durations for the *Rhododendron cf brachycarpum* point cloud 36

ACRONYMS

3D	: Three-dimensional
ALIA	: Average Leaf Inclination Angle
API	: Application Programming Interface
ASCII	: American Standard Code for Information Interchange
BSI CMOS	: Backside-Illuminated Complementary Metal-Oxide-Semiconductor
CBD	: Convention on Biological Diversity
CPU	: Central Processing Unit
DBH	: Diameter at Breast Height
DHP	: Digital Hemispherical Photography
EBV	: Essential Biodiversity Variables
EU	: European Union
GB	: Gigabyte
GEO BON	: Group on Earth Observations Biodiversity Observation Network
GHz	: Gigahertz
LAD	: Leaf Angle Distribution
LAI	: Leaf Area Index
LAIe	: Effective Leaf Area Index
LDP	: Levelled Digital Photography
LIA	: Leaf Inclination Angle
LiDAR	: Light Detection and Ranging
LTS	: Long-Term Support
NR	: Number of Replicates
PCD	: Point Cloud Data
PCL	: Point Cloud Library
PDF	: Probability Density Function
PTX	: Point Cloud Data eXchange
RAM	: Random Access Memory
SD	: Standard Deviation
SDGs	: Sustainable Development Goals
SSD	: Solid State Drive
TLS	: Terrestrial Laser Scanning
TLSLeAF	: Terrestrial Laser Scanning Leaf Angle Function
UHD	: Ultra High Definition

1. INTRODUCTION

1.1. Background

The accumulating body of evidence of accelerating global biodiversity loss has stimulated regional and worldwide responses through platforms that include the United Nations Sustainable Development Goals (SDGs), the Convention on Biological Diversity (CBD) (Pereira et al., 2013; Skidmore et al., 2021) and more recently, the European Union's (EU) Biodiversity Strategy for 2030 (European Union, 2020). Essential Biodiversity Variables (EBVs) were formulated by the Group on Earth Observations Biodiversity Observation Network (GEO BON) as crucial measurements for studying, reporting, and management of biodiversity change (Pereira et al., 2013). Six EBV classes include genetic composition, species populations, species traits, community composition, ecosystem function, and ecosystem structure (Pereira et al., 2013). The gap between biodiversity monitoring initiatives and policymakers can be bridged through EBVs by determining the state and trends of biodiversity (Geijzendorffer et al., 2016). EBVs generation is conducted by integrating primary observations or field data with remote sensing (Skidmore et al., 2021).

Light interception is essential in estimating canopy productivity (Niinemets, 2010). Plants seek to optimise light harvesting by increasing total leaf area or enhancing the effectiveness of light interception per unit leaf area (Raabe et al., 2015). However, shading may limit leaf exposure, thus lowering the productivity potential (Niinemets and Fleck, 2002). Plants adjust their leaf angles to improve light transmission, enhancing light availability throughout their vertical canopy profile (Niinemets, 2010; Raabe et al., 2015). Vegetation canopies are usually described through structural parameters, one regarding leaf amount and characterised through leaf area index (LAI), while the other is about leaf orientation, denoted through leaf angle distribution (LAD) (Zhao et al., 2015).

1.2. Leaf Area Index

LAI is a biophysical trait of vegetation that informs the EBV classes of ecosystem structure and ecosystem function (García-Haro et al., 2018). It is the one-sided total green leaf area per unit of horizontal ground surface area (Chen and Black, 1992). Ground-based techniques of estimating LAI have been grouped into direct and indirect approaches (Jonckheere et al., 2004). Estimating LAI through direct methods comprises the destructive sampling of leaves, litterfall collection and point contact sampling (Zhao et al., 2011; Zheng and Moskal, 2009). Direct methods have been reported to be highly accurate, albeit with the disadvantages of being destructive to vegetation, laborious and time-consuming, limiting their spatial and temporal application (Jonckheere et al., 2004; Xu et al., 2018; Yan et al., 2019). Indirect methods quantify LAI through measurements of other variables, such as light transmission through vegetation canopies or gap fraction and radiative transfer models (Colaizzi et al., 2017; Yan et al., 2019; Zheng and Moskal, 2009). These methods have the advantages of being generally quicker, non-destructive, and adaptable to automation and are thus widely used for more extensive spatial sampling (Hu et al., 2018; Jonckheere et al., 2004; Mu et al., 2017). Examples of indirect methods include the point quadrat approach, the use of ceptometers, digital hemispherical photography (DHP), laser scanning, and multispectral imaging (Zhao et al., 2019). These different tools apply the same physical principle, the gap fraction theory, to model the interactions between light and vegetation (Fournier and Hall, 2017; Yan et al., 2019). The gap fraction method has been widely explored and used compared to other approaches due to its established theory and functional and efficient measurement schemes for continuous canopies (Hu et al., 2018). Remote

sensing techniques, based on airborne or spaceborne platforms, have also been applied in determining LAI and are based on the differences in the spectral reflectance between vegetation and other land cover types (Jonckheere et al., 2004). These remote sensing methods facilitate coverage of large spatial extents non-destructively but require calibration using independent in situ LAI measurements (Colaizzi et al., 2017).

1.3. The G-Function

The gap fraction theory estimates LAI through gap probability or gap size distribution based on the Beer-Lambert law (Hu et al., 2018; Yan et al., 2019). Gap fraction illustrates the likelihood of transmitting a beam of light in the direction θ through a horizontally homogenous canopy without interception and is determined by the foliage amount and orientation (i.e., LAI and $G(\theta)$, respectively) (Zhao et al., 2019) as denoted by Nilson, (1971):

$$P(\theta) = e^{-G(\theta).LAIe/\cos\theta} \quad (1)$$

where $P(\theta)$ is the gap probability of the light beam penetrating the canopy without being intercepted, LAIe is the effective Leaf Area Index (LAI), and $G(\theta)$ represents the 'G-function', defined as the projection coefficient of unit foliage area onto a plane perpendicular to the viewing direction (Ross, 1981). Eq. 1 can be used to indirectly estimate the effective LAI instead of the true LAI since the model assumes random spatial distribution of foliage; without considering the overlapping and clumping of leaves (Zheng and Moskal, 2009). The non-random distribution of canopy foliage, overlapping and clumping of leaves, and the presence of non-photosynthetic materials make it difficult to obtain the true LAI from indirect methods, despite efforts to eliminate some of the effects through methods such as the gap size theory (Chen and Cihlar, 1996; Zheng and Moskal, 2009). However, true LAI can be obtained through direct harvesting methods such as destructive sampling, which are also used for validation of indirect methods (Jonckheere et al., 2004; Weiss et al., 2004).

The influence of LAD on light transmission through a canopy and thus on indirect LAI quantification through gap fraction was established as early as the 1950s, leading to the introduction of the leaf projection function G to represent this influence (Monsi and Saeki, 1953, 2005; Monteith, 1965; Wang et al., 2007; Yan et al., 2019). LAD comprises the leaf inclination and the leaf azimuthal angles, which are respectively defined as the angle between the zenith and the leaf surface normal (Ross, 1981) and the clockwise angle between the principal axis projection of vegetation foliage on the horizontal plane and the north direction (Lugg et al., 1981). The leaf azimuthal angle is commonly assumed to be uniform; thus, G can be denoted as (Wang et al., 2007; Wilson, 1960, 1967):

$$G(\theta) = \int_0^{\pi/2} A(\theta, \theta_L) f(\theta, \theta_L) d\theta_L \quad (2)$$

$$A(\theta, \theta_L) = \begin{cases} \cos\theta \cos\theta_L, & and\ |\cot\theta \cot\theta_L| > 1 \\ \cos\theta \cos\theta_L [1 + (2/\pi)(\tan\psi - \psi)], & and\ |\cot\theta \cot\theta_L| \leq 1 \end{cases} \quad (3)$$

where $\psi = \cos^{-1}(\cot\theta \cot\theta_L)$, θ is the incoming beam zenith angle, and θ_L is the leaf zenith angle. G has been shown to directly impact gap fraction at various viewing angles, with gap probabilities varying significantly at different zenith angles and LAD types (Yan et al., 2019).

The estimation of LAD has been carried out via either direct or indirect methods (Li et al., 2018; Xu et al., 2018). Direct geometrical methods comprise devices such as a clinometer (Gratani and Ghia, 2002) and a

simple device made up of a ruler, protractor, and compass (Norman and Campbell, 1989) to quantify leaf angle distribution. Lang (1973) developed a mechanical instrument made up of high-precision potentiometers with three protruding arms which can measure the coordinates of any point on a leaf by recording the angular information of the three arms. These approaches are based on observing individual leaves to acquire a representative description of the whole canopy (Norman and Campbell, 1989). Direct measurements can produce highly accurate results but are laborious and time-consuming (Daughtry, 1990). The precise determination of LAD with these methods also depends on physical contact with the plants, which could lead to disturbance and possible damage to the foliage or limited access due to complexities in the canopy structure (Zheng and Moskal, 2012). Furthermore, a larger quantity of leaves (e.g., at least 100) should be used to estimate the LAD, and the leaves in higher canopy positions are not always easy to reach (Itakura and Hosoi, 2019).

Indirect methods are based on observing how a canopy attenuates sunlight at different view angles (Norman and Campbell, 1989; Wagner and Hagemeier, 2006). LAD can then be estimated by inverting Beer's law for radiation interception (Norman and Campbell, 1989). However, separating the effect of leaf angles on canopy transmittance from other structural influences, such as woody material, is difficult with these methods (Chen et al., 1991; Zou et al., 2014). Ryu et al. (2010) introduced a robust but affordable indirect method that entails the manual identification of leaf angles from levelled digital photography (LDP) of canopies comprised of flat leaves. The method facilitates a rapid, non-contact and highly accurate estimation of LAD (Ryu et al., 2010) and has been validated as a suitable way to overcome the shortcomings of direct methods (Pisek et al., 2011). However, this photographic method only considers leaves in direct view, approximately perpendicular to the camera's viewing direction (Ryu et al., 2010). The technique is also challenging to automate, and significant user interaction is required to identify appropriate leaves for inclination angle measurement (Raabe et al., 2015).

1.4. Research Gap and Scientific Contribution

Terrestrial laser scanning (TLS) instruments have been increasing use when acquiring measurements from the canopy structure (Hosoi and Omasa, 2006; Yang et al., 2013). TLS instruments are ground-based devices that use light detection and ranging (LiDAR) to measure the distance to a target based on the time recorded between the emission of laser pulses and their return (Kissling et al., 2022; Koma et al., 2021). These instruments also facilitate field data collection to obtain species trait information for individual plants (Kissling et al., 2018). The advantages of TLS include high angular resolution and robust anti-interference capability (Hu et al., 2018; Xu et al., 2018). TLS has been used to provide detailed vegetation structure information such as the diameter at breast height (DBH) (Liu et al., 2018), leaf area index (LAI) (Zheng et al., 2013), tree height (Kalwar et al., 2016; Wezyk et al., 2007), above-ground biomass (Demol et al., 2022; Gonzalez de Tanago et al., 2018), and crown structure (Bayer et al., 2013). Various methods have been proposed for retrieving LAD information from LiDAR data (e.g., Hosoi and Omasa, 2006; Zheng and Moskal, 2012; Jin et al., 2016; Zhao et al., 2015; Bailey and Mahaffee, 2017; Li et al., 2018; Liu et al., 2019; Vicari et al., 2019; Stovall et al., 2021), yet no intercomparison has been reported so far.

Remote sensing biodiversity products can be converted into EBVs or biodiversity change indicators through the integration of data from various technologies such as LiDAR; this technology is enormously powerful for extracting three-dimensional (3D) habitat structures (Skidmore et al., 2021). Standardised, open, accessible, repeatable and reproducible measurements and processing procedures during the extraction of trait data are critical for reliable biodiversity monitoring (Kissling et al., 2018; Skidmore et al., 2021). This study aims to conduct the intercomparison of different methods published in literature on LAD estimation for broadleaf tree species with TLS data and calibrating output from the LAD algorithms against the known LAD from a 'standard' simulated tree.

The thesis contributes towards the identification of a plausible, standardised approach for determining leaf inclination angle distributions with TLS in the field, which is a required benchmark to validate plant function trait indicators proposed for the EU's Biodiversity Strategy for 2030 of nature protection and restoration and similar programmes (EC, 2020).

1.5. Problem Statement

Overall, LAD is considered integral to spectral reflectance and radiation transmission properties of vegetation canopies, and hence interception, absorption, evapotranspiration, and photosynthesis (Asner, 1998; Myneni et al., 1989; Niinemets, 2010; Ross, 1981; Stuckens et al., 2009; Utsugi et al., 2006). LAD is a fundamental parameter of models that illustrate the energy and mass exchanges for vegetation at all scales (Li et al., 2018; Vicari et al., 2019). It has been considered an essential variable in canopy productivity and rainfall interception modelling (Xiao et al., 2000). Plants adjust leaf angle to acquire resources such as light or adapt to environmental changes (Darwin, 1881; Ehleringer and Forseth, 1980; Muraoka et al., 1998). Moreover, the leaf inclination angle can indicate plant stress, such as water deficiency, severe heat or a disease (Konishi et al., 2009; Omasa et al., 2007). However, challenges in measuring LAD have caused it to be one of the most poorly characterised parameters (Ollinger, 2011). It is typically presumed to be random or simplified using predefined mathematical functions without considering its variation (Liu et al., 2019; Vicari et al., 2019).

1.6. Research Objectives and Questions

1.6.1. Main Research Objective

This study aims to test, compare, and evaluate the performance of available TLS-based LAD estimation methods using terrestrial LiDAR data.

1.6.2. Specific Research Objectives

The specific objectives of this study are:
Objective 1: To compare the available LAD estimation techniques using TLS point clouds of both real and synthetic trees covering the full range of the existing LAD types.
Objective 2: To evaluate the performance of the proposed TLS-based methods using the established LDP approach (Ryu et al., 2010; Pisek et al., 2011).

1.6.3. Research Questions

Question 1: Is there an agreement between the independent methods in retrieving LAD information from LiDAR data? (Specific to objective 1).
Question 2: What are the strengths and limitations of the methods used to extract LAD information from LiDAR data? (Specific to objective 2).
Question 3: What might be the recommendations for improving LAD retrieval with LiDAR data in the future? (Specific to objectives 1 and 2).

2. STUDY AREA, DATA, AND ALGORITHMS

2.1. Study Areas

This study comprises two study areas to enhance the possibility of the TLS point clouds of the selected real trees covering the full range of the existing LAD types.

2.1.1. Royal Botanic Gardens, Kew

The first study area for this research is the Royal Botanic Gardens at Kew, London, England, depicted in Figure 1. The garden was established in 1759 and is located within latitudes 51° 28'20" N - 51° 28'40" N and longitudes 0° 17'50" E - 0° 18'10" E. It is approximately 320 acres in size, with at least 16,900 plant species from all over the world and is also known as the Kew Gardens (*Royal Botanic Gardens, Kew | Kew*).

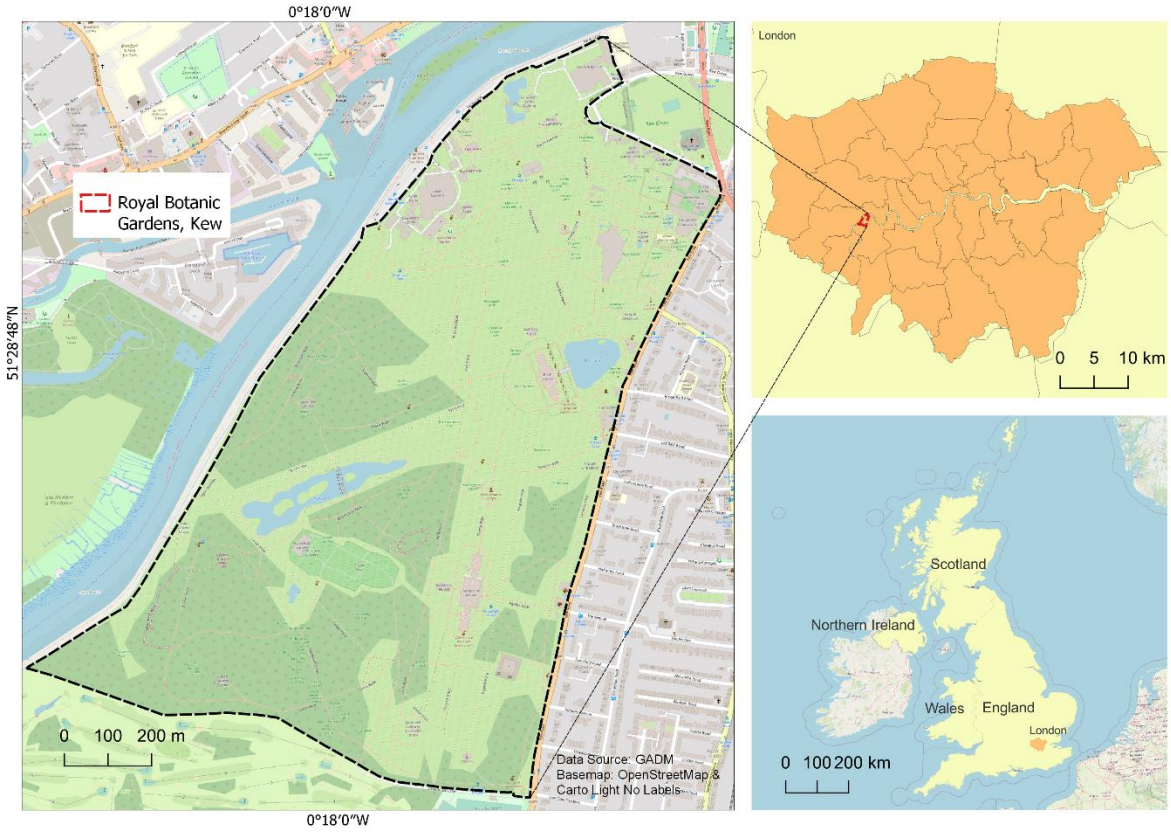

Figure 1: Location map of the Royal Botanic Gardens at Kew

2.1.2. Kumpula Botanic Garden

The Kumpula Botanic Garden (Figure 2) is in Jyrängöntie, Helsinki, Finland. The garden has two sections: the garden of cultivated plants and the geobotanical garden. The garden of cultivated plants contains various species used for economic and ornamental purposes (*Kumpula Botanic Garden | LUOMUS*).

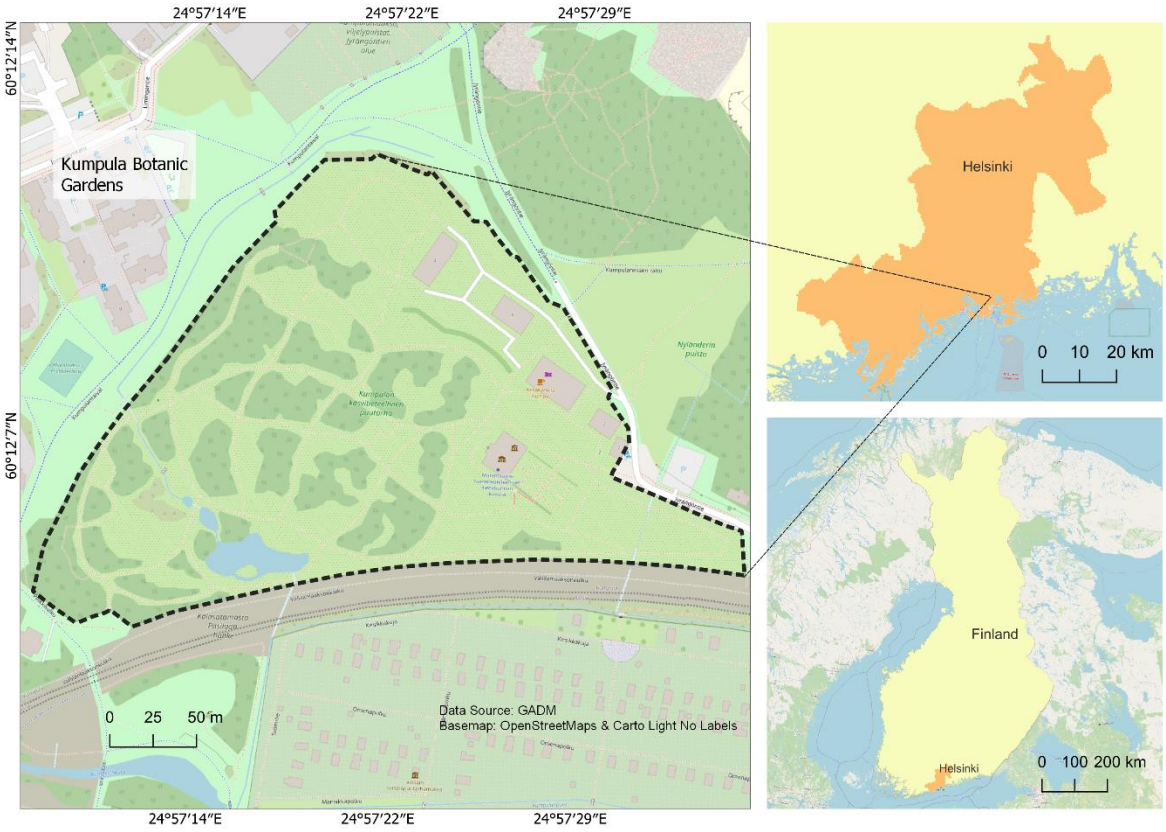

Figure 2: Location map of the Kumpula Botanic Garden

2.2. Algorithms and Data

2.2.1. LAD Estimation Algorithms

This study evaluates the following TLS-based LAD estimation techniques introduced by Zheng and Moskal (2012), Bailey and Mahafee (2017), Liu et al. (2019), Vicari et al. (2019), Stovall et al. (2021) and the Point Cloud Library (PCL normals estimation) (*Point Cloud Library*). The source codes used by Zheng and Moskal (2012), Bailey and Mahafee (2017), Liu et al. (2019), Vicari et al. (2019), and Stovall et al. (2021) were acquired from the respective authors. Point Cloud Library is an online, open-source project for point cloud processing.

Zheng and Moskal (2012) applied a total least squares fitting technique to reconstruct leaf normal vectors by fitting a plane to its six neighbouring LiDAR leaf intersection points. In their study, Zheng and Moskal (2012) reported good performance of their algorithm in estimating the angular variability of a small plant or seedling, with a 78.51% accuracy. However, in the same study, a prediction accuracy of 57.28% indicated less agreement for a mature tree in its natural environment. The algorithm is based on the Computational Geometry Algorithms Library (CGAL). This open-source C++ library grants easy access to efficient and reliable geometric algorithms, such as the estimation of normals (*The Computational Geometry Algorithms Library*).

Bailey and Mahafee (2017) developed an LAD estimation method based on the triangulation of LiDAR leaf intersection points that directly calculates the normal vector of the plane formed by three adjacent points. The method also involves weighting of triangles before generating a probability density function for leaf orientation from triangle normal vectors. This weighting was intended to prevent a substantial

results bias towards the TLS scanner (Bailey and Mahaffee, 2017). The algorithm is based on the Helios simulation system, a flexible modelling framework that utilises a C++ API to handle tasks like managing geometry and associated data structures (*Helios Documentation v1.2.58*).

Liu et al. (2019) sought to improve the estimation of LAD from TLS by considering the leaf size constraint. They initially classified point clouds based on geometric and radiometric attributes, separating leaves from woody material to facilitate the retrieval of LAD without the effects of the non-photosynthetic material (Liu et al., 2019). The algorithm is based on Python 3 and uses the classified leaf point clouds to reconstruct leaf surfaces through plane fitting constrained by the leaf size parameter.

Vicari et al. (2019) introduced a threshold based on the covariance matrix of neighbourhood points to eliminate points with significant errors from the estimated LAD. The algorithm is based on Python 2. It initially conducts the Nearest Neighbours search around every point in a leaf-only point cloud for nearby points that are then used in the estimation of leaf normals. The algorithm further deems it essential to strike a balance between having a number of neighbouring points small enough to lessen the probability of angles calculated from more than a single leaf and having an adequate number of points to decrease the effect of data noise (Vicari et al., 2019).

Stovall et al. (2021) developed Terrestrial Laser Scanning Leaf Angle Function (TLSLeAF), an algorithm that calculates LAD from gridded point clouds. The algorithm is based on the R language and has a built-in feature that classifies wood and leaves. TLSLeAF calculates leaf normals directly from the gridded TLS point clouds. The computation of the LAD is with respect to the horizon in the point cloud grid direct from the leaf surface normals (Stovall et al., 2021).

The PCL is a standalone, large-scale, open-source project designed for the purpose of processing 2D/3D images and point clouds (*Point Cloud Library*). PCL has prebuilt binaries for Linux, Windows, and MacOS. Given a geometric surface, the Point Cloud Library normals estimation feature directly computes surface normals at each point in the cloud (*Point Cloud Library*).

Table 1 summarises the publications and their corresponding abbreviated names, which will be used as references throughout this study for conciseness.

Table 1: A summary of the publications and their corresponding shorter naming used in this study for reference

LAD Estimation Method	***Abbreviated name***
Bailey and Mahafee (2017)	Bailey
Liu et al. (2019)	Liu
Stovall et al. (2021)	TLSLeAF
Zheng and Moskal (2012)	Zheng
Point Cloud Library	PCL

2.2.2. TLS field data

Real tree LiDAR data from the Royal Botanic Gardens at Kew were acquired on October 17th 2017, using a 3D RIEGL VZ-400 portable laser scanner. The scanner offers a measurement range of around 700 m, a 1550nm wavelength and a beam divergence of 0.35 milliradians. An angular resolution of 0.04º

was used. A tripod was used to support the scanner at a position that was 1.5 m above the ground, and measurements were taken from four different positions, roughly 5 metres from each tree. Individual tree species that were scanned included a date plum (*Diospyros lotus*), the maidenhair tree (*Ginkgo biloba*), the Japanese hop hornbeam (*Ostrya japonica*), and the Wollemi pine (*Wollemia nobilis*).

TLS point clouds from the Kumpula Botanic Garden were collected on October 12th, 2021, using a Leica P40 Scan Station. The scanner has a laser with a 405nm wavelength, a range of close to 270 metres, and a beam divergence of 0.23 milliradians. The trees of interest were scanned from four different positions. They included the common pear (*Pyrus communis 'Olga'*), the European oak (*Quercus robur*), the Himalayan rosebay (*Rhododendron cf branchycarpum*) and the European beech (*Fagus sylvatica*).

2.2.3. Simulated TLS data

3D synthetic tree models were generated using Arbaro, an open-source software based on geometrical observables to produce and style three-dimensional trees for replicating natural scenery (Weber and Penn, 1995). The artificial trees were further edited in Blender 3.4 (*Foundation Blender*). These models were then 'scanned' using a simulation system to generate simulated LiDAR data of the models.

2.2.4. LDP field data

The levelled digital photography method (Ryu et al., 2010) was applied in the study areas under calm conditions to minimise the effects of wind on leaves (Tadrist et al., 2014). The cameras used were an Apple iPhone SE2020 with a 12-megapixel f/1.8 aperture wide camera and a Sony Xperia Z5 Compact phone with a 23-megapixel 1/2.3-inch multi-aspect BSI CMOS sensor, along with an F2.0 lens, both hand-balanced (based on the observer's judgement). The distortion of the camera lenses has not been established so far. The LDP method has been shown to provide consistent results with direct leaf angle measurements (Pisek et al., 2011).

3. METHODOLOGY

This section provides the study's methodology to assess and compare various LAD estimation methods, as outlined in the Figure 3 flowchart. The following subsections outline the key steps involved in the methodology, including data pre-processing, algorithm implementation, and statistical analysis.

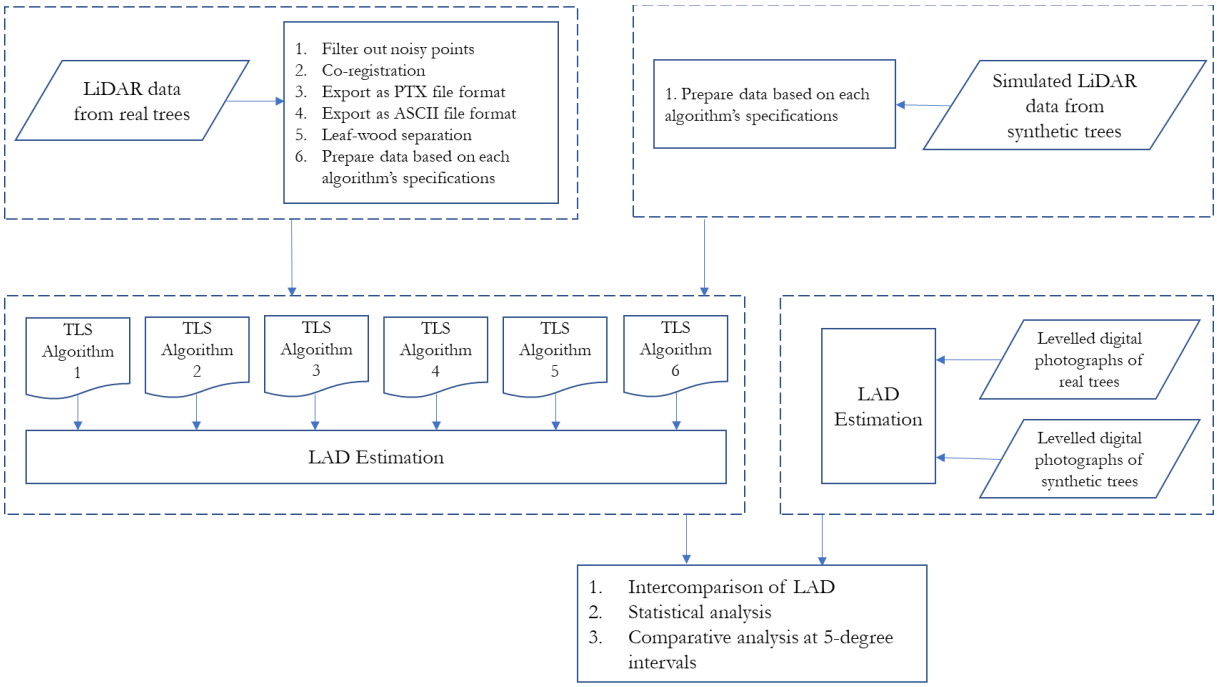

Figure 3: The overall study workflow

3.1. Data Pre-processing

First, filtering was performed using the RiScan Pro software to remove noisy points from the real LiDAR data and retain only high-confidence range values based on the pulse shape deviation (Pfennigbauer and Ullrich, 2010). Co-registration was also conducted to align the multiple scans. The trees of interest were manually extracted from the co-registered point clouds using CloudCompare software. The TLS data was further prepared based on the specific requirements of each LAD estimation algorithm. First, as individual scans for each tree, the data was exported from RiScan Pro as gridded TLS scan point clouds (PTX format), an input file format required for the TLSLeAF algorithm (Stovall et al., 2021). Second, individual scans were exported into an American Standard Code for Information Interchange (ASCII) file format (.XYZ), and parameters for each scan were specified in a separate metadata file to facilitate data processing for the method proposed by Bailey and Mahaffee (2017). TLS scans of each tree species were also merged for the following approaches: Zheng and Moskal (2012), Vicari et al. (2019), Liu et al. (2019) and the Point Cloud Library. The merged scans were also converted into the PCD (Point Cloud Data) file format, specifically for the Point Cloud Library.

3.2. Leaf-wood Separation

The TLSLeAF algorithm has an inbuilt feature that separates leaves from wood using supervised classification (random forest) based on multiscale normal estimates (Stovall et al., 2021). However, with the other algorithms not possessing a similar feature, the leaf-wood separation of the real TLS scans was conducted using a Python package called TLSeparation. The TLSeparation package is a leaf-wood

classification package for TLS data that performs unsupervised classification based on geometric features and shortest path analysis (Vicari, 2017). Leaves were separated from the wood in the synthetic, simulated 3D object using Aspose.3D assets extractor (*Aspose.3D Product Family*), an open-source application used to separate embedded meshes and textures from OBJ files.

3.3. Estimation of Leaf Inclination Angles

Different algorithms require setting various parameters to facilitate the process of LAD computation. The Vicari algorithm had a fixed number of neighbouring points (kNN) for each particular point set. Lmax values, representing the radius of the neighbourhood distance in executing the leaf constraint in Liu and a pre-set threshold length for comparison with triangle sides in Bailey, were set, respectively. TLSLeAF also involves setup options, such as the threshold of scattering angle, topographic normalisation of voxels, scales for normal computation, voxel resolution for LAD normalisation, and the minimum number of measurements per voxel.

The subsequent TLS data, prepared based on each method's requirements, was added to each algorithm's pipeline to estimate the leaf normals and/or leaf inclination angles (LIAs). TLSLeAF, Liu, and Vicari provide the LIA directly, while the output of the other algorithms is leaf normal vectors. Leaf angles were thus calculated in degrees using:

$$\alpha = \cos^{-1}\frac{\vec{N}.\vec{z}}{|\vec{N}||\vec{z}|}\ X\ \frac{180}{\pi} \tag{4}$$

where $\vec{N}$ represents the normal vector and $\vec{z}$ is the zenith vector.

The estimation of leaf angles using TLS-based algorithms was performed on a Lenovo Thinkpad P15s Gen 1 laptop equipped with an Intel(R) Core i7-10610U CPU @ 1.80GHz 2.30 GHz processor. This machine also had Windows 10 Pro 64 and Ubuntu Linux LTS (Version 20.04) operating systems. The laptop featured a maximum memory capacity of 48GB 2667MHz DDR4-2666 RAM and 512GB solid-state drive (SSD) storage. The computing setup had both a dedicated graphics card and integrated graphics. It included a 2GB NVIDIA Quadro P520 graphics card, as well as Intel UHD Graphics. Five algorithms were tested within the Windows operating system during the leaf angle estimation process, while the PCL algorithm was executed on the Ubuntu Linux LTS system.

3.4. Leaf Inclination Angle Distribution

The resulting leaf inclination angles from the algorithms were fitted with the two-parameter Beta distribution function (Goel and Strebel, 1984). This function was reported as best suited for the description of the probability density function of the leaf angle distribution (Wang et al., 2007):

$$f(t) = \frac{1}{B(\mu,\upsilon)}\ (1-t)^{\mu-1}t^{\upsilon-1} \tag{5}$$

where μ and υ represent the two beta distribution parameters, θ_L is the leaf inclination angle in radians, $t = 2\theta_L/\pi$, while $B(\mu,\upsilon)$ denotes the Beta-distribution function, further described as:

$$B(\mu,\upsilon) = \int_0^1 (1-x)^{\mu-1}x^{\upsilon-1}dx = \frac{\Gamma(\mu)\Gamma(\upsilon)}{\Gamma(\mu+\upsilon)} \tag{6}$$

where Γ represents the Gamma function. The two parameters, μ and υ, can be computed in relation to the mean $\bar{t}$ by:

$$\upsilon = \bar{t}\left(\frac{\sigma_0^2}{\sigma_t^2} - 1\right) \quad (7)$$

$$\mu = \left(1 - \bar{t}\right)\left(\frac{\sigma_0^2}{\sigma_t^2} - 1\right) \quad (8)$$

where σ_0^2 is the maximum standard deviation of t, obtained through $\sigma_0^2 = \bar{t}(1 - \bar{t})$, whereas σ_t^2 is the variance of t (Wang et al., 2007).

The distribution of leaf inclination angles can be described using the six common functions proposed by De Wit (1965) (Figure 4) that are based on empirical evidence and mathematical considerations (Chianucci et al., 2018; Raabe et al., 2015). These functions include uniform, planophile, plagiophile, erectophile, extremophile, and spherical. Uniform canopies have an equal proportion of leaf inclination angles at any angle; planophile canopies are characterised by horizontally oriented leaves; plagiophile canopies by inclined leaves; erectophile canopies by vertically oriented leaves; extremophile canopies have a high frequency of both horizontally and vertically oriented leaves, and in spherical canopies, the relative frequency of leaf inclination angles is the same as that for a sphere (Lemeur and Blad, 1974).

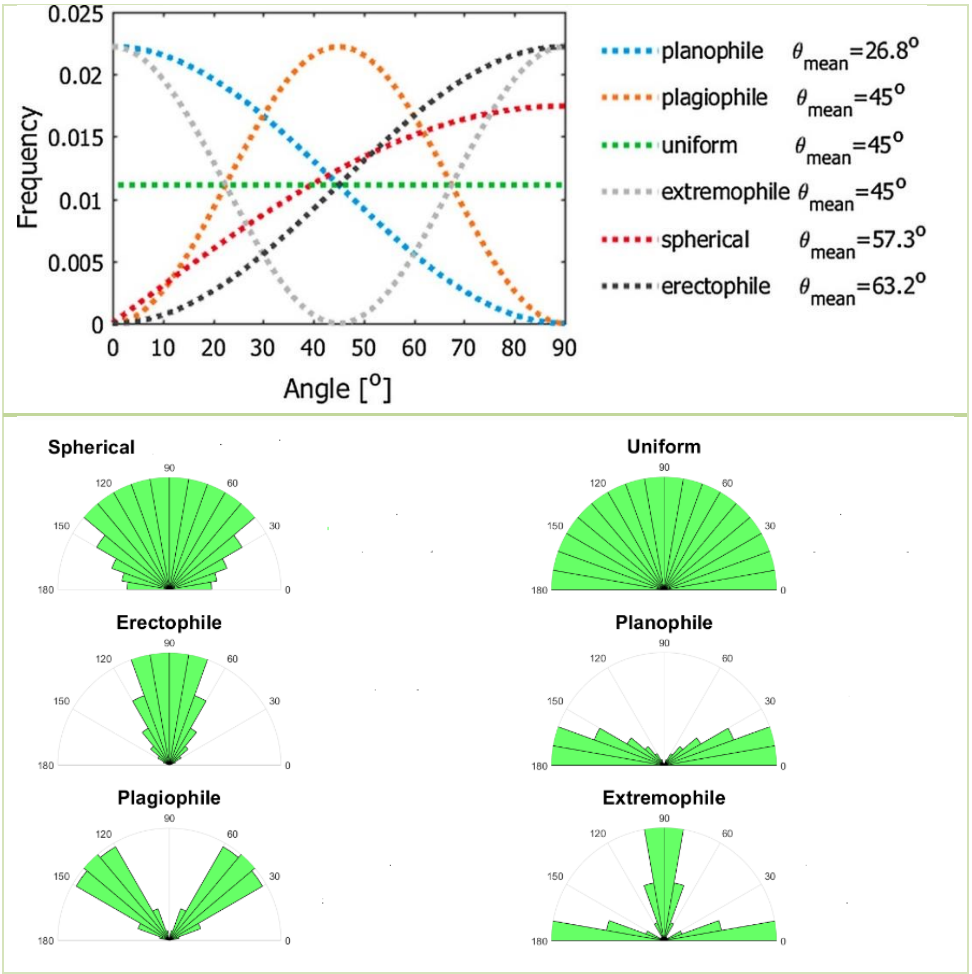

Figure 4: The six classical predefined mathematical functions by De Wit (1965). Credit: Liu et al., 2019 and Canopy — SCOPE 1.8 Documentation, respectively.

The classical distributions are extensively utilised and offer a more straightforward interpretation than the beta distribution's parameter values. The measured distributions of leaf inclination angles ($f(\theta_L)$) were categorised by identifying the most similar classical distribution type. To calculate the difference from the distributions proposed by De Wit (1965) $f_{deWit}(\theta_L)$, a modified inclination index developed by Ross (1975) was applied to each leaf inclination angle distribution:

$$X_L = \int_0^{\frac{\pi}{2}} |f(\theta_L) - f_{deWit}(\theta_L)| d\theta_L \quad (9)$$

The measured LADs were then assigned to the class that returned the lowest X_L score.

3.5. Statistical Analysis

Statistical tests were carried out to assess the level of agreement between the leaf angle distributions obtained from the six TLS algorithms, including the reference LDP approach. With the algorithms potentially predicting a variety of LAD types, the tests were conducted using the Mann-Whitney U-Test, a non-parametric test which assumes no particular distribution (McKnight and Najab, 2010). The tests were executed using R-Studio 2022.07.2, and pairwise matrices were generated to facilitate inter-comparison between the algorithms.

3.6. Generation of 3D Synthetic Trees

The Arbaro software provides a method for defining the characteristics of tree elements based on the traits of their parent element (Weber and Penn, 1995). To generate synthetic trees using this software, the first step involved defining the geometric shape of the tree, which determines the branch length as it extends from the trunk at different heights. For example, a tree with a conical shape would have larger branches closer to the bottom of the trunk. The next stage was to determine the number of levels in the tree, which determines the number of sub-branches that a branch or sub-branch can have. In this study, a specific configuration was set that included creating the trunk, branches, sub-branches, and leaves. The number of branches and sub-branches and their degrees of curvature, angle and radius were defined relative to the entire tree. Afterwards, the shape, size, and quantity of leaves were specified. Arbaro adjusts the orientation of the leaves by identifying their location and normal vector in tree coordinates (Weber and Penn, 1995). The software then calculates the existing and desired angles to align the leaves accordingly. Thus, Leaf orientation adjustments were made to ensure that the 3D models obtained the required LAD types for the study. The artificial trees were further edited with Blender, another open-source software, to ensure that the leaves and their normals faced outward and to facilitate the acquisition of the leaf normal coordinates. The generated leaves were flat without any curvature.

3.7. Performance Evaluation of LAD Estimation Methods

Simulated datasets were used in evaluating the consistency and performance of the leaf angle estimation approaches based on the fact that each simulated leaf's location and true angle were known beforehand. This approach is similar to those used in previous research (Bailey and Mahaffee, 2017; Liu et al., 2019; Zheng and Moskal, 2012). The Helios simulation system, a flexible modelling framework that can perform various tasks, including managing geometry and related data structures via a C++ API (*Helios Documentation v1.2.58*), was used in the virtual scanning of the 3D models' leaves.

The virtual scanner was positioned 1.5 m above the ground. The scan origins were specified for eight different positions surrounding the 3D models to ensure complete coverage. Figure 5 outlines parameters

that define the overall scan for one scanner position. The 'ASCII_format' tag defines the column format of the output ASCII file; origin refers to the position of the virtual scanner; size refers to the scan resolution in terms of the number of points in the zenithal and azimuthal directions; thetaMin and thetaMax represent the range of the scan zenithal angle, while phiMin and phiMax denote the range of the scan's rotation in the azimuthal direction (*Helios Documentation v1.2.58*).

```
<helios>

    <scan>
        <ASCII_format> x y z r255 g255 b255 </ASCII_format>
        <origin> 1.0 25.5 1.5 </origin>
        <size> 8500 10500 </size>
        <thetaMin> 30 </thetaMin>
        <thetaMax> 130 </thetaMax>
        <phiMin> 0 </phiMin>
        <phiMax> 360 </phiMax>
    </scan>

<helios>
```

Figure 5: A sample of the synthetic scan metadata for one scanner position

The resulting high-resolution synthetic scans were used with five TLS algorithms, excluding TLSLeAF. TLSLeAF relies on gridded point cloud data to estimate leaf angles, whereas the simulated datasets could only be generated in an ASCII file format. Screenshots of the 3D models were also taken to facilitate LAD estimation using the LDP approach.

A statistical analysis involving testing the results of the 6 LAD estimation methods against the synthetic model using the non-parametric Mann-Whitney U-test was conducted. This test aimed to determine if there was a statistically significant difference between each method and the artificial model. Additionally, a comparative analysis was performed to generate figures that compared the LAD of the synthetic model with the LAD obtained from each approach using the simulated point clouds at 5-degree intervals. To achieve this, a normality test was performed at each 5-degree interval to assess the distribution of the data. If the data was found to be normally distributed, a parametric t-test was conducted. Conversely, a non-parametric Mann-Whitney U-test was used if the data was not normally distributed. Following the statistical test, a plot was generated to visualise the results. If a statistically significant difference was detected, a shaded region was included in the plot to represent the difference. The shaded areas served as visual indicators of the statistical significance, helping to highlight any deviations between the synthetic model's LAD and the LAD obtained from each algorithm.

4. RESULTS

This section provides the findings of the study based on the proposed methodology. The results of the inter-comparison of LAD estimates from the LAD estimation approaches for real trees are presented. Moreover, the results of statistical tests to assess the level of agreement amongst the different approaches and the assessment of the performance of the techniques based on synthetic data are illustrated.

4.1. LAD Estimation of Real Trees with TLS and LDP

This section presents the LAD results for the trees of interest using three components. First, an image of the real trees captured in the two study areas is included, allowing for visual inspection and identification of individual trees. Second, a graph compares the distribution of leaf inclination angles against the leaf angle frequency for the six different TLS algorithms and the reference LDP approach. This graph provides an overview of the performance of each method in estimating the distribution of leaf angles. A table then summarises each method's performance in estimating the LAD for each tree of interest.

4.1.1. Kumpula Botanic Garden

Most TLS algorithms predominantly classified the LAD type for the *Pyrus communis 'Olga'* tree shown in Figure 6(a) as erectophile, with the Bailey and TLSLeAF algorithms opting for a spherical LAD, as shown in Figure 6(b) and Table 2. The range between the highest and lowest ALIA values for the TLS algorithms was approximately 14.31°, with the standard deviation being comparable amongst the algorithms. Most algorithms were consistent with the reference LDP method in finding an erectophile LAD type. The TLS algorithms demonstrated a high number of leaf normal replicates, ranging from 783,775 to 5,083,496, primarily due to the utilisation of point clouds with a high sampling resolution for estimating leaf normal vectors in TLS (Vicari et al., 2019; Zheng and Moskal, 2012). The TLSLeAF algorithm, described by Stovall et al. (2021), utilises gridded point clouds to estimate multiple angles for each leaf. The Vicari algorithm works under the assumption that LAD can be retrieved by obtaining all valid planes fitted to the points in a leaf point cloud (Vicari et al., 2019). In contrast to the TLS algorithms, the LDP approach employed a considerably lower number of replicates, precisely 78. The LDP method involves manually selecting specific leaves for analysis and subsequently measuring the leaf angle inclination for each chosen leaf, resulting in one leaf normal replication per leaf (Pisek et al., 2011).

Table 2: Statistical results of the LAD retrieval methods for the Pyrus communis 'Olga' (i.e., the average leaf inclination angle in degrees (ALIA), standard deviation (SD), two parameters (μ and ν), LAD type based on De Wit (1965) (Distribution) and the number of normals' replicates (NR)).

Algorithm	*ALIA(°)*	*SD*	*μ*	*ν*	*Distribution*	*NR*
Bailey	57.1	22.25	1.02	1.77	spherical	2123801
Liu	71.41	19.72	0.50	1.91	erectophile	5082338
PCL	69.55	16.68	0.93	3.18	erectophile	5082520
TLSLeAF	55.72	19.31	1.57	2.55	spherical	4003057
Vicari	63.39	19.70	0.99	2.36	erectophile	783775
Zheng	67.47	17.73	0.96	2.87	erectophile	5083496
LDP	68.69	20.05	0.62	2.01	erectophile	78

Next, the *Quercus robur*, shown in Figure 7(a), displayed an agreement of the spherical LAD type by all the TLS algorithms, with a range of 7.11° between the maximum and minimum ALIA values (Table 3). However, the Liu algorithm showed a different leaf angle frequency compared to the other TLS

algorithms, as demonstrated in Figure 7(b), with its standard deviation also higher than the consistent range from the other algorithms. Though it indicated the lowest ALIA compared to the TLS approaches, the reference LDP method was consistent with the TLS algorithms' findings in identifying a spherical LAD type, as depicted in Table 3.

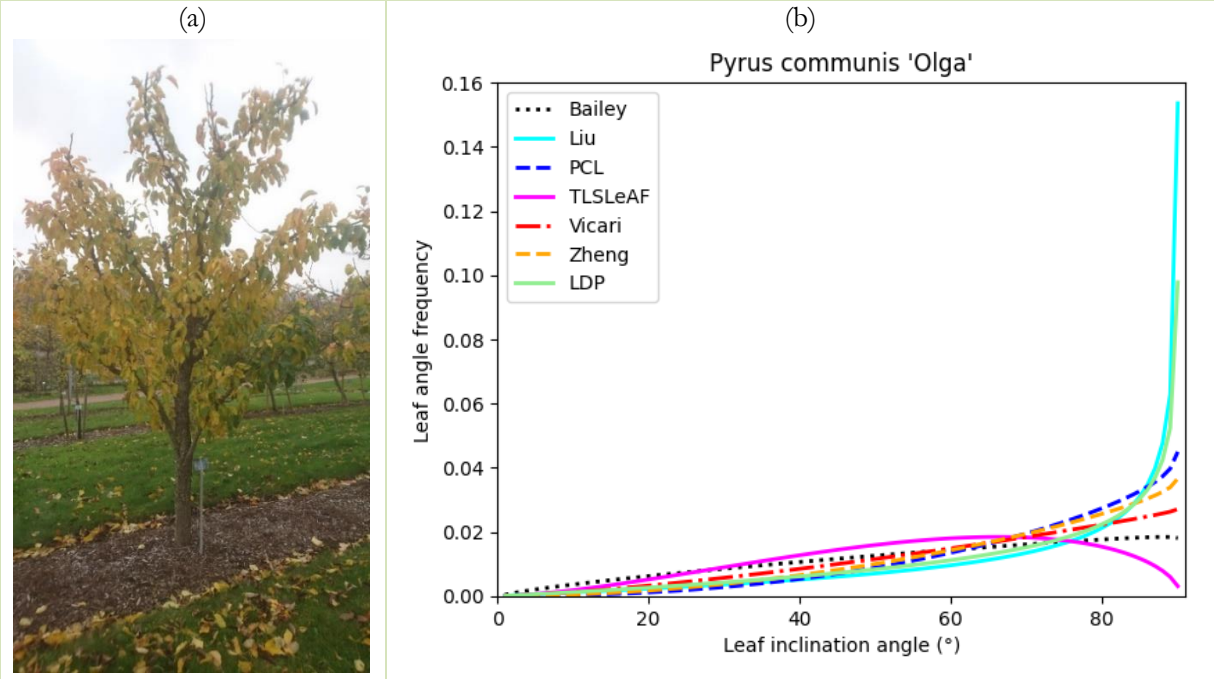

Figure 6: (a) An image of Pyrus communis 'Olga' (b) Fitted beta distributions of leaf inclination angles for Pyrus communis 'Olga' for each TLS algorithm and the LDP approach.

Table 3: Statistical results for the LAD retrieval methods for Quercus robur (i.e., the average leaf inclination angle in degrees (ALIA), standard deviation (SD), two parameters (μ and ν), LAD type based on De Wit (1965) (Distribution) and the number of leaf normal replicates (NR)).

Algorithm	***ALIA(°)***	***SD***	***μ***	***ν***	***Distribution***	***NR***
Bailey	54.46	21.84	1.21	1.85	spherical	1758680
Liu	59.31	26.33	0.55	1.07	spherical	5140721
PCL	57.01	20.84	1.22	2.11	spherical	5139379
TLSLeAF	52.20	19.56	1.74	2.41	spherical	3728297
Vicari	58.44	20.35	1.21	2.24	spherical	1925924
Zheng	58.20	20.62	1.19	2.17	spherical	5150274
LDP	51.19	21.47	1.43	1.88	spherical	129

The scanned *Rhododendron cf branchycarpum* shrub tree exhibited drooping (wilting) leaves, as shown in Figure 8(a). Among the six TLS algorithms examined, the majority (four out of six) identified the tree's LAD type as erectophile. However, Bailey and TLSLeAF suggested a spherical LAD, as indicated in Table 4. Notably, a range of 10.36° was observed between the maximum and minimum values of the ALIA estimated by the different TLS approaches. The LDP method aligned with the minority by indicating a spherical LAD for the tree.

For the *Fagus sylvatica* (Figure 9(a)), all TLS algorithms agreed on the spherical LAD type (Table 5). The consistency among the TLS algorithms is noteworthy, with each algorithm indicating a spherical LAD for this species. The range of ALIA values between the minimum and maximum estimates from the TLS approaches was 6.58°. However, the Liu algorithm again exhibited a distinct PDF pattern compared to the

other TLS algorithms (Figure 9(b)). In contrast to the TLS algorithms, the LDP method suggested a plagiophile LAD type for the *Fagus sylvatica*, with its PDF pattern and ALIA value differing from most of the TLS algorithms.

7(a)

7(b)

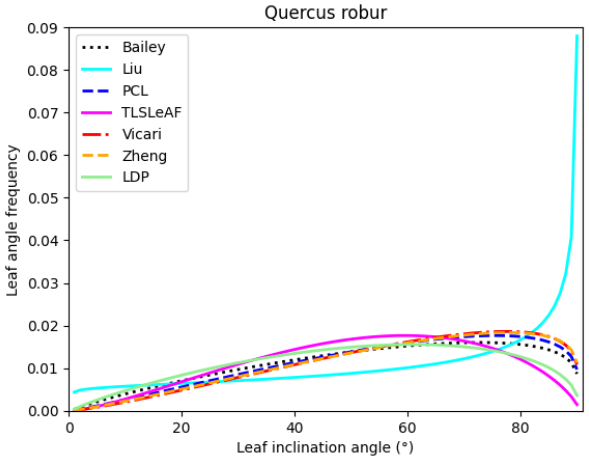

Figure 7: (a) An image of Quercus robur (b) Fitted beta distributions of leaf inclination angles for Quercus robur for each TLS algorithm and the LDP approach

8(a)

8(b)

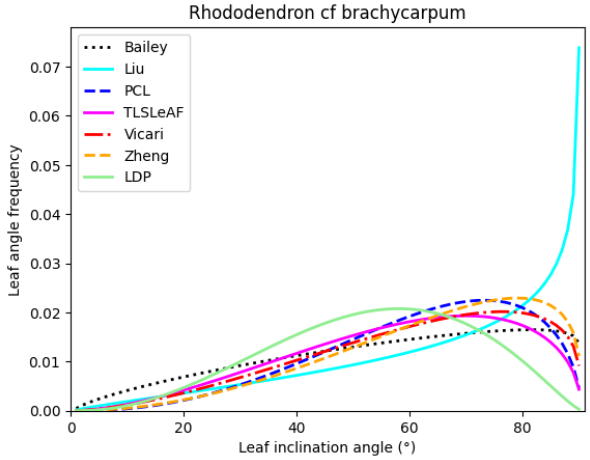

Figure 8: (a) An image of Rhododendron cf branchycarpum (b) Fitted beta distributions of LIAs for Rhododendron cf branchycarpum

Table 4: Statistical results for the LAD retrieval methods for Rhododendron cf branchycarpum (i.e., the average leaf inclination angle in degrees (ALIA), standard deviation (SD), two parameters (μ and ν), LAD type based on De Wit (1965) (Distribution) and the number of leaf normal replicates (NR)).

Algorithm	***ALIA(°)***	***SD***	***μ***	***ν***	***Distribution***	***NR***
Bailey	55.41	22.45	1.08	1.73	spherical	1496229
Liu	65.77	21.29	0.68	1.84	erectophile	3752621
PCL	61.58	17.12	1.57	3.40	erectophile	3752471
TLSLeAF	57.71	18.95	1.50	2.69	spherical	3998834
Vicari	60.17	19.10	1.30	2.62	erectophile	864441
Zheng	63.21	17.77	1.30	3.07	erectophile	3753702
LDP	53.10	17.22	2.30	3.31	spherical	86

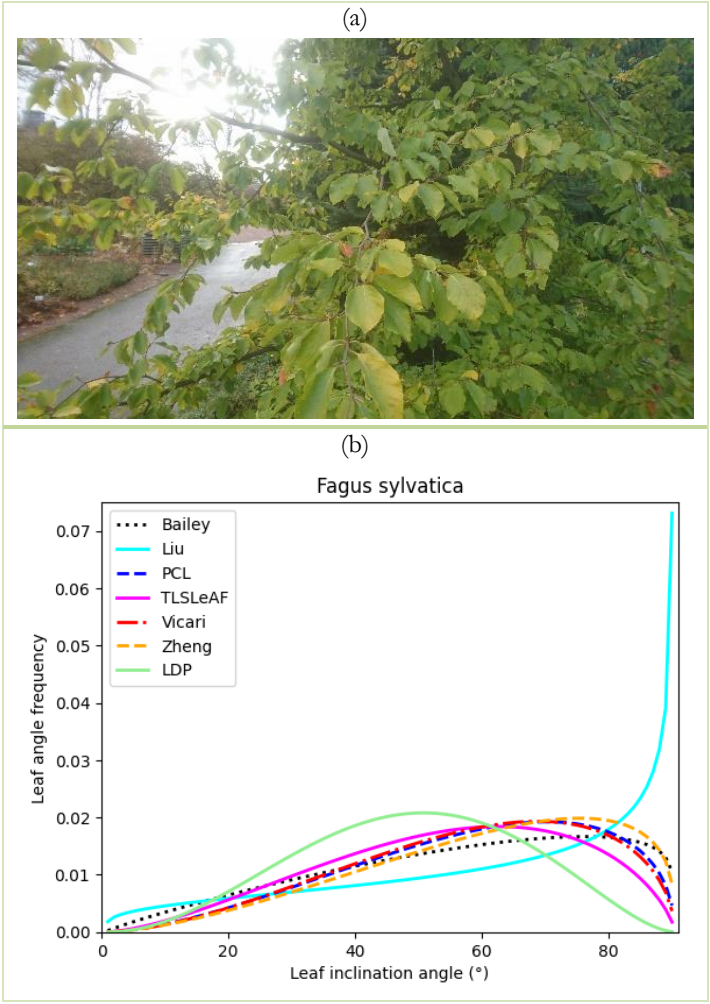

Figure 9: (a) An image of Fagus sylvatica (b) Fitted beta distributions of LIAs for Fagus sylvatica

Table 5: Statistical results for the LAD retrieval methods for Fagus sylvatica (i.e., the average leaf inclination angle in degrees (ALIA), standard deviation (SD), two parameters (μ and ν), LAD type based on De Wit (1965) (Distribution) and the number of leaf normal replicates (NR)).

Algorithm	***ALIA(°)***	***SD***	***μ***	***ν***	***Distribution***	***NR***
Bailey	55.6	21.68	1.17	1.9	spherical	3409206
Liu	60.79	24.74	0.62	1.28	spherical	9286541
PCL	57.83	19.04	1.48	2.66	spherical	9286334
TLSLeAF	54.21	19.10	1.72	2.60	spherical	8997463
Vicari	57.44	18.81	1.55	2.73	spherical	2632255
Zheng	59.66	19.17	1.32	2.60	spherical	9294361
LDP	48.47	17.05	2.73	3.19	plagiophile	125

4.1.2. Kew Botanic Garden

Figure 10(a) shows the scanned *Wollemia nobilis* tree. Most algorithms agreed on a uniform LAD type for the tree, except the TLSLeAF, which suggested a spherical LAD (Table 6). Despite portraying a different LAD type, the pattern of the PDF for TLSLeAF was consistent with most of the approaches (Figure 10(b)). The LDP approach aligned with most TLS algorithms in identifying the uniform LAD type estimation and the PDF pattern. However, the Liu algorithm depicted an inverted PDF pattern compared to the other approaches, with its standard deviation value being notably higher than the rest. As expected,

the TLS-based algorithms continued to involve a high number of normal replicates in their estimation of LAD, as compared to the LDP approach.

Table 6: Statistical results for the LAD retrieval methods for Wollemia nobilis (i.e., the average leaf inclination angle in degrees (ALIA), standard deviation (SD), two parameters (μ and ν), LAD type based on De Wit (1965) (Distribution) and the number of leaf normal replicates (NR)).

Algorithm	***ALIA(°)***	***SD***	***μ***	***ν***	***Distribution***	***NR***
Bailey	47.79	22.89	1.34	1.51	uniform	453612
Liu	45.40	27.16	0.86	0.88	uniform	744902
PCL	45.43	21.88	1.60	1.63	uniform	746278
TLSLeAF	49.74	21.79	1.44	1.78	spherical	1084722
Vicari	43.96	22.09	1.61	1.54	uniform	431365
Zheng	46.49	22.34	1.48	1.58	uniform	746409
LDP	46.71	22.05	1.52	1.64	uniform	80

The *Ginkgo biloba* leaves displayed wilting characteristics, as shown in Figure 11(a). The Bailey, Liu, and TLSLeAF algorithms indicated a spherical LAD type in their LAD estimation for the tree. In contrast, the other three algorithms suggested an erectophile LAD type, as shown in Figure 11(b) and Table 7. The LDP method aligned with the spherical LAD type. The TLSLeAF, unlike the other TLS algorithms, registered an ALIA value that was 9.49º lower than the closest TLS algorithm.

10(a)

10(b)

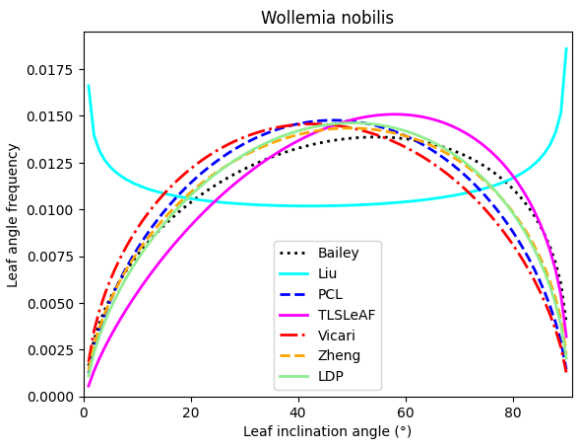

Figure 10: (a) An image of Wollemia nobilis (b) Fitted beta distributions of LIAs for the Wollemia nobilis

11(a)

11(b)

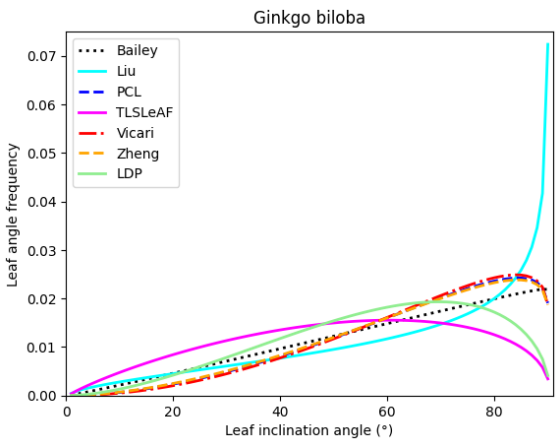

Figure 11: (a) An image of Ginkgo biloba (b) Fitted beta distributions of LIAs for Ginkgo biloba

Table 7: Statistical results for the LAD retrieval methods for Ginkgo biloba (i.e., the average leaf inclination angle in degrees (ALIA), standard deviation (SD), two parameters (μ and ν), LAD type based on De Wit (1965) (Distribution) and the number of leaf normal replicates (NR)).

Algorithm	***ALIA(°)***	***SD***	***M***	***ν***	***Distribution***	***NR***
Bailey	60.38	20.94	1.01	2.06	spherical	317707
Liu	63.80	22.65	0.66	1.60	spherical	550153
PCL	64.27	18.29	1.13	2.82	erectophile	550787
TLSLeAF	50.89	21.46	1.44	1.88	spherical	592273
Vicari	64.84	17.84	1.15	2.97	erectophile	415402
Zheng	63.92	18.45	1.13	2.77	erectophile	550809
LDP	57.67	18.90	1.52	2.70	spherical	78

Figure 12(a) shows the image of the scanned *Ostrya japonica* tree, where leaves showed noticeable drooping. A similar pattern to the *Ginkgo biloba* tree emerged in the LAD estimation of this species. The Bailey, Liu, and TLSLeAF algorithms once again suggested a spherical LAD type, while the other three algorithms indicated an erectophile LAD type, as shown in Figure 12(b) and Table 8. However, unlike for *Ginkgo biloba*, the LDP method settled for the erectophile LAD type. TLSLeAF returned a lower ALIA value than the other TLS algorithms, consistent with its estimation of *Ginkgo biloba's* LAD (Table 7).

Table 8: Statistical results for the LAD retrieval methods for Ostrya japonica (i.e., the average leaf inclination angle in degrees (ALIA), standard deviation (SD), two parameters (μ and ν), LAD type based on De Wit (1965) (Distribution) and the number of leaf normal replicates (NR)).

Algorithm	***ALIA(°)***	***SD***	***M***	***ν***	***Distribution***	***NR***
Bailey	58.49	21.33	1.07	1.98	spherical	252231
Liu	59.50	25.30	0.62	1.21	spherical	391003
PCL	61.16	18.75	1.29	2.73	erectophile	391260
TLSLeAF	53.51	20.70	1.44	2.12	spherical	331822
Vicari	62.18	18.65	1.23	2.75	erectophile	245306
Zheng	62.07	18.91	1.19	2.65	erectophile	391279
LDP	66.37	11.63	2.78	7.81	erectophile	90

A similar trend with the *Ginkgo biloba* and *Ostrya japonica* arose with the *Diospyros lotus* (Figure 13(a)). The Bailey, Liu, and TLSLeAF algorithms suggested a spherical LAD type, while the PCL, Vicari and Zheng algorithms indicated a plagiophile LAD type (Table 9). The Liu algorithm generally agreed with the other TLS algorithms, as Figure 13(b) shows through its PDF pattern. Although the TLS algorithms differed in their LAD types, the range of the ALIA between them was only 1.16°. This difference suggests a relatively small variation in the estimated leaf angles among the TLS algorithms. On the other hand, the LDP approach agreed with the TLS algorithms that suggested an erectophile LAD type. However, the ALIA and SD estimated by the LDP method were noticeably lower than those obtained from the TLS algorithms (Table 9). This discrepancy is evident in the PDF representation of the LDP approach in Figure 13(b).

Table 9: Statistical results for the LAD retrieval methods for Diospyros lotus (i.e., the average leaf inclination angle in degrees (ALIA), standard deviation (SD), two parameters (μ and ν), LAD type based on De Wit (1965) (Distribution) and the number of leaf normal replicates (NR)).

Algorithm	*ALIA(°)*	*SD*	*M*	*ν*	*Distribution*	*NR*
Bailey	52.05	19.54	1.76	2.41	spherical	238518
Liu	52.76	21.61	1.33	1.88	spherical	479766
PCL	52.45	16.72	2.52	3.52	plagiophile	480615
TLSLeAF	51.77	20.21	1.63	2.21	spherical	714156
Vicari	51.95	16.09	2.80	3.83	plagiophile	354563
Zheng	52.93	16.98	2.39	3.41	plagiophile	480642
LDP	39.59	11.00	8.68	6.82	plagiophile	100

12(a)

12(b)

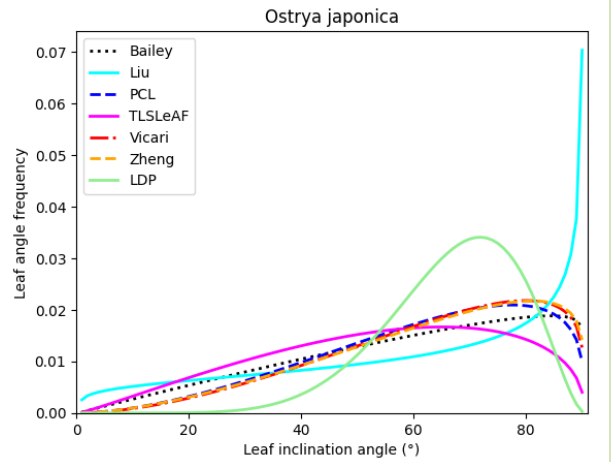

Figure 12: (a) An image of Ostrya japonica. (b) Fitted beta distributions of LIAs for Ostrya japonica.

13(a)

13(b)

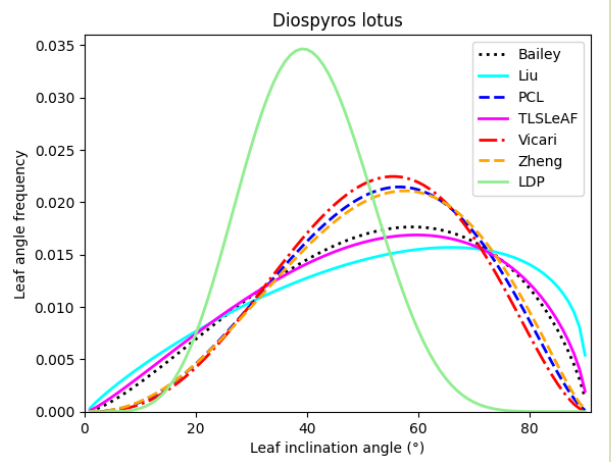

Figure 13: (a) An image of Diospyros lotus. (b) Fitted beta distributions of LIAs for Diospyros lotus.

4.2. Statistical Analysis

In this study, we aimed to investigate whether the algorithms exhibited significant differences in their estimation of leaf angles or were consistent in producing similar LAD results. Section 4.3 highlights whether each algorithm showed significant differences when compared to a simulated tree with a known characterisation of a specific LAD type. The Mann-Whitney U test was chosen as the appropriate confirmatory statistical test. Tables 10 and 11 present the results of the Mann-Whitney U-test for the six TLS algorithms, including the LDP approach. The test was evaluated with a significance level of 0.05 for the Kumpula and Kew Gardens' trees. The cells highlighted in light red indicate that the p-value is less

than the significance level, suggesting a statistically significant difference between the leaf angle distributions (LADs) of the compared pair of algorithms. Conversely, cells highlighted in light green represent p-values greater than 0.05, indicating no statistically significant difference between the LADs of the compared algorithms.

In Table 10, statistically significant differences were observed between TLSLeAF and PCL regarding the LAD of the *Pyrus communis 'Olga'*. Similarly, the Liu algorithm exhibited disagreement with Bailey, TLSLeAF, and Vicari while aligning with the remaining methods. Additionally, the LDP method concurred with all TLS algorithms except for Bailey and TLSLeAF. For the estimation of LAD in *Quercus robur*, all LAD approaches displayed agreement, with Liu differing from all methods except Vicari and Zheng. *Rhododendron cf brachycarpum* and *Fagus sylvatica* demonstrated similar outcomes, where all LAD estimation methods reached an agreement, except for two cases in which the Liu algorithm disagreed with both Bailey and TLSLeAF.

Table 10: Pairwise comparison of P-values from the Mann-Whitney U-test for the trees at the Kumpula Botanic Garden. Cells highlighted in light red indicate p-values < 0.05, while those in light green represent p-values > 0.05.

Pyrus communis olga

	Bailey	PCL	TLSLeAF	Vicari	Zheng	Liu	LDP
Bailey	1						
PCL	0.0565	1					
TLSLeAF	0.6919	0.0322	1				
Vicari	0.6400	0.2495	0.5489	1			
Zheng	0.1774	0.6400	0.1241	0.5225	1		
Liu	0.0005	0.8648	0.0001	0.0427	0.3995	1	
LDP	0.0114	0.7025	0.0027	0.2025	0.8134	0.4306	1

Quercus robur

	Bailey	PCL	TLSLeAF	Vicari	Zheng	Liu	LDP
Bailey	1						
PCL	0.4306	1					
TLSLeAF	0.3652	0.3314	1				
Vicari	0.4718	0.6835	0.4124	1			
Zheng	0.4771	0.7089	0.3979	0.8514	1		
Liu	0.0080	0.0476	0.0019	0.1020	0.0879	1	
LDP	0.5662	0.3713	0.5114	0.4323	0.4272	0.0039	1

Rhododendron cf brachycarpum

	Bailey	PCL	TLSLeAF	Vicari	Zheng	Liu	LDP
Bailey	1						
PCL	0.9327	1					
TLSLeAF	0.4631	0.9327	1				
Vicari	0.6116	0.8626	0.5720	1			
Zheng	0.9350	0.8851	0.9396	0.8784	1		
Liu	0.0341	0.5759	0.0193	0.2519	0.5956	1	
LDP	0.6626	0.8491	0.6359	0.8693	0.8536	0.3187	1

Fagus sylvatica

	Bailey	PCL	TLSLeAF	Vicari	Zheng	Liu	LDP
Bailey	1						
PCL	0.5114	1					
TLSLeAF	0.3343	0.4206	1				
Vicari	0.5170	0.9601	0.4239	1			
Zheng	0.5740	0.8068	0.5300	0.8045	1		
Liu	0.0466	0.2301	0.0113	0.2323	0.3091	1	
LDP	0.6730	0.7562	0.6626	0.7562	0.8112	0.4373	1

All LAD estimation methods for the Kew Gardens species were consistent with the estimation of the LAD of the *Wollemia nobilis* without significant differences, except for the Liu algorithm (Table 11). A complete agreement was observed for the LAD estimation of the *Ginkgo biloba* across all approaches, except where Liu and TLSLeAF diverged. Similar trends were observed for *Ostrya japonica*, mirroring the results of *Ginkgo biloba*, where all TLS algorithms displayed agreement except for one case (Liu and TLSLeAF). However, unlike with the *Ginkgo biloba*, the LDP method aligned with only PCL, Vicari, and Zheng for the *Ostrya japonica*. For the LAD estimation of *Diospyros lotus*, all TLS methods agreed. However, the LDP approach again only agreed with PCL, Vicari and Zheng, as shown in Table 11.

Table 11: Pairwise comparison of P-values from the Mann-Whitney U-test for the trees at the Royal Botanic Garden at Kew. Cells highlighted in light red indicate p-values < 0.05, while those in light green represent p-values > 0.05.

Wollemia nobilis

	Bailey	PCL	TLSLeAF	Vicari	Zheng	Liu	LDP
Bailey	1						
PCL	0.2117	1					
TLSLeAF	0.1563	0.5413	1				
Vicari	0.2590	0.6523	0.4011	1			
Zheng	0.3458	0.4492	0.2931	0.6156	1		
Liu	0.0146	0.0275	0.0307	0.0241	0.0189	1	
LDP	0.2368	0.7238	0.4289	0.8648	0.5375	0.0254	1

Ginkgo biloba

	Bailey	PCL	TLSLeAF	Vicari	Zheng	Liu	LDP
Bailey	1						
PCL	0.8648	1					
TLSLeAF	0.9966	0.6919	1				
Vicari	0.7825	0.9943	0.6056	1			
Zheng	0.9032	0.9738	0.7454	0.9989	1		
Liu	0.2701	0.8290	0.0269	0.9578	0.7628	1	
LDP	0.9738	0.9783	0.4492	0.8896	0.9943	0.2213	1

Ostrya japonica

	Bailey	PCL	TLSLeAF	Vicari	Zheng	Liu	LDP
Bailey	1						
PCL	0.7847	1					
TLSLeAF	0.6983	0.6983	1				
Vicari	0.8716	0.8716	0.8312	1			
Zheng	0.8738	0.8603	0.8514	0.9783	1		
Liu	0.1783	0.5078	0.0472	0.6543	0.6298	1	
LDP	0.0395	0.0917	0.0336	0.0973	0.0901	0.0304	1

Diospyros lotus

	Bailey	PCL	TLSLeAF	Vicari	Zheng	Liu	LDP
Bailey	1						
PCL	0.7367	1					
TLSLeAF	0.6136	0.7454	1				
Vicari	0.8738	0.8784	0.9010	1			
Zheng	0.7089	0.8874	0.7025	0.8648	1		
Liu	0.3806	0.7346	0.4190	0.9032	0.6856	1	
LDP	0.0361	0.1063	0.0281	0.1357	0.0939	0.0212	1

4.3. Performance Evaluation of Algorithms with Synthetic Data

Three 3D models with spherical, uniform and erectophile LAD types were used to validate the performance of the algorithms. Figures 14 (a) and (b) show a sample 3D model with spherical LAD and a version of the same model with leaves only, respectively. The models were generated with flat leaves with no curvature; thus, a closer agreement was expected between the LDP approach and the TLS methods.

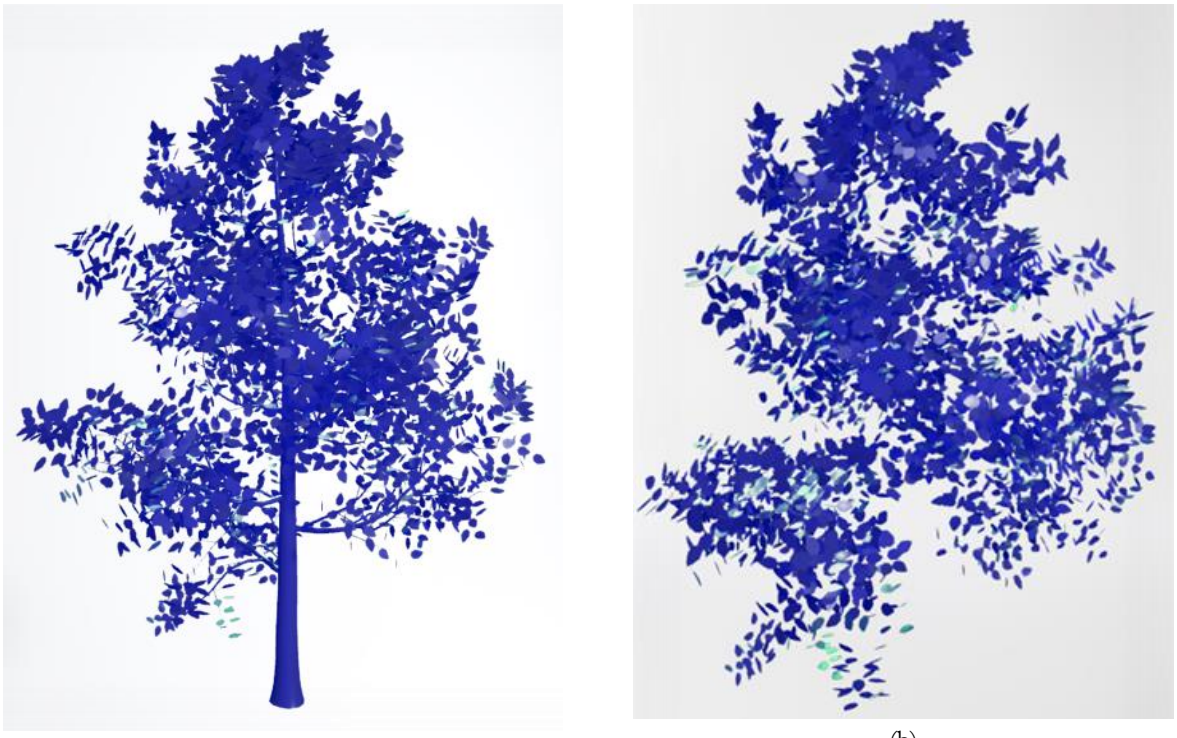

(a) (b)

Figure 14: (a) A 3D model of a synthetic tree with spherical LAD. (b) A leaf-only 3D model of the same synthetic tree.

4.3.1. Spherical Synthetic Data LAD

The results indicate that the LAD estimation approaches showed a spherical LAD type consistent with the simulated synthetic tree model. Bailey, PCL, Vicari, and Zheng returned ALIA values within a ±1.5° range

of the synthetic model's value. However, the Liu algorithm had higher ALIA and SD values, suggesting it overestimated the LIA, as shown in Figure 15, where most of the LAD estimation approaches relatively agree, except for the Liu algorithm. This outcome by the Liu algorithm is consistent with the algorithm's less robust performance (see section 4.1) for most of the real trees.

Table 12: Statistical results (The average leaf inclination angle (ALIA), standard deviation (SD), two parameters μ, ν, LAD type (Distribution) based on De Wit (1965), and the number of leaf normal replicates (NR)) from the LAD estimation approaches based on a simulated, spherical LAD, tree representation.

Algorithm	***ALIA***	***SD***	***μ***	***ν***	***Distribution***	***NR***
Synthetic model	56.86	21.65	1.11	1.91	spherical	7908
Bailey	55.67	22.24	1.09	1.77	spherical	492085
Liu	61.00	25.08	0.58	1.23	spherical	1213369
PCL	56.85	21.75	1.1	1.88	spherical	1213547
Vicari	56.57	21.91	1.09	1.85	spherical	1190793
Zheng	56.52	21.89	1.1	1.85	spherical	1213548
LDP	52.16	22.62	1.2	1.66	spherical	231

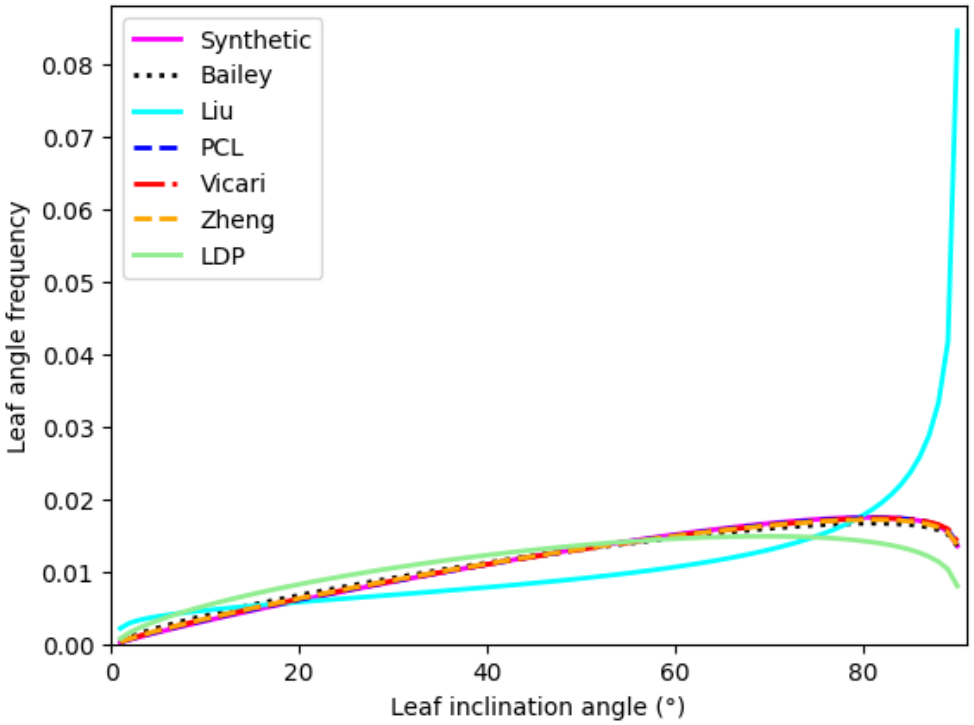

Figure 15: Fitted beta distributions of LIAs for the simulated spherical LAD tree representation.

The results of the non-parametric Mann-Whitney U-test to assess the level of agreement between the LAD estimation approaches and the synthetic spherical LAD tree representation are presented in Table 13. The results show no statistically significant difference between the LAD estimation approaches and the synthetic model at the 5% significance level. Specifically, all algorithms had p-values greater than 0.05, with the Liu algorithm having a p-value of 0.050002, marginally above the threshold.

The comparative analysis between the spherical LAD synthetic model and each LAD estimation method at 5-degree intervals is presented in Figure 16. The Bailey algorithm exhibited statistically significant differences highlighted by the shaded areas, specifically at 10º-25º and 60º-85º, while showing agreement

with the synthetic model at the other angles. The Liu algorithm, on the other hand, displayed significant differences with the model throughout, except at two 5-degree intervals. Notably, the PCL algorithm showed agreement with the synthetic model across all angles. The Zheng and Vicari algorithms demonstrated similar agreements with the synthetic model, with discrepancies observed only between 70º-80º for Vicari and 70º-85º for Zheng. Lastly, the LDP method exhibited statistically significant differences with the model, only agreeing at one 5-degree section.

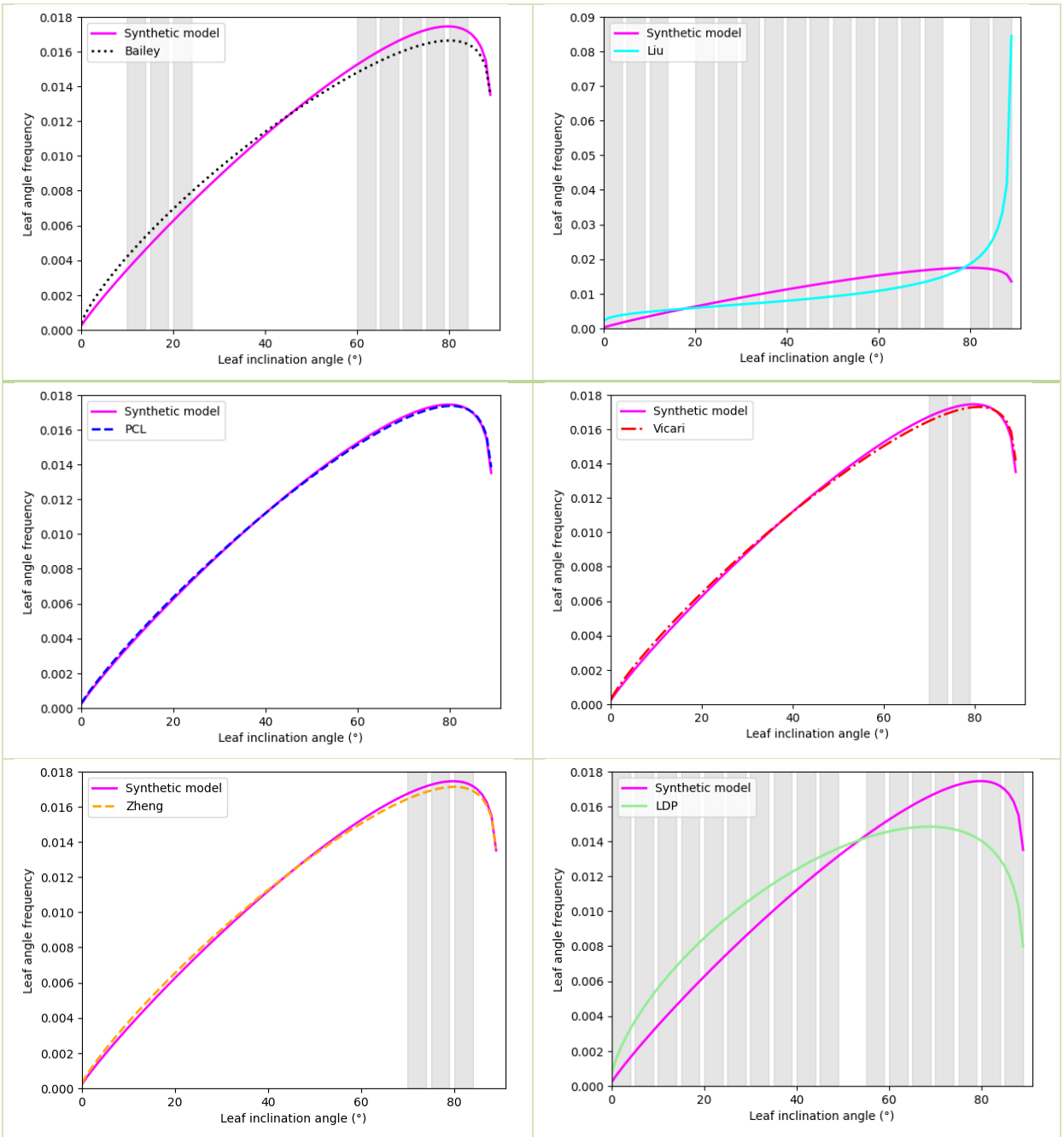

Figure 16: Comparative analysis results for the synthetic spherical TLS dataset at 5-degree intervals, with shaded regions indicating a statistically significant difference between the synthetic model and the LAD estimation method.

Table 13: P-value results of LAD estimation approaches against the synthetic spherical, uniform and erectophile LAD tree representations.

Algorithm	***Spherical LAD***	***Uniform LAD***	***Erectophile LAD***
Bailey	0.6434	0.3064	0.9697
Liu	0.0500	1.73E-06	0.8450
PCL	0.9383	0.6334	0.9921
Vicari	0.8538	0.3993	0.9921
Zheng	0.8077	0.3807	0.9921
LDP	0.3993	0.1370	0.8981

4.3.2. Uniform Synthetic Data LAD

The LAD estimation approaches for the synthetic uniform tree representation show that, except for the Liu algorithm, all methods agreed on a uniform LAD type, as indicated in Table 14. In contrast to the synthetic spherical tree representation, there was a wider range of ALIA values when the LAD estimation methods were compared to the synthetic uniform model. The LDP approach had the lowest ALIA value, closest to the synthetic model's value. On the other hand, the Liu algorithm exhibited the highest ALIA value and showed a significant difference in its PDF compared to the other methods, as shown in Figure 17.

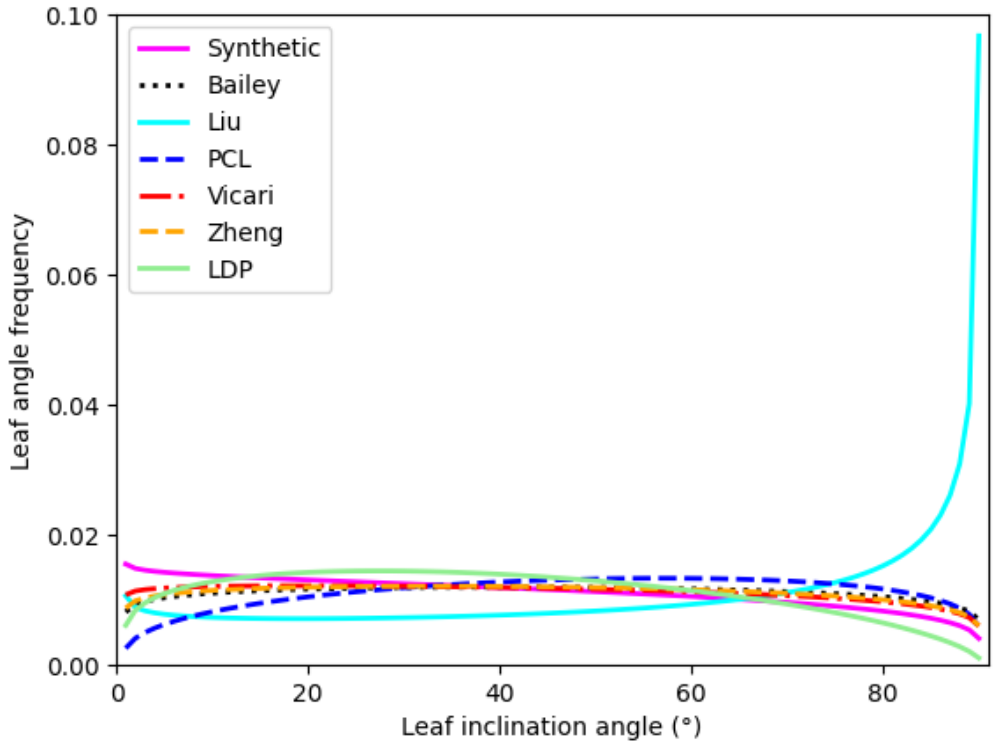

Figure 17: Fitted beta distributions of LIAs for the simulated uniform LAD tree representation.

The p-value results between the LAD estimation approaches, and the uniform LAD synthetic tree model between the LAD estimation approaches and the uniform LAD synthetic model at the 5% level of significance are shown in Table 13. Specifically, the Liu algorithm had a significantly low p-value (< 0.001), indicating a significant difference from the synthetic model compared to the other methods. In contrast, all other algorithms had p-values greater than 0.05, indicating no significant difference from the model.

In contrast to the comparative analysis conducted between the spherical LAD synthetic model and each LAD estimation method at 5-degree intervals, the analysis performed with the uniform synthetic model revealed a more significant number of disagreements, as depicted in Figure 18's shaded regions. In this analysis, all the algorithms displayed agreement with the synthetic model only at points where their respective line graphs intersected, except for the Liu algorithm, which did not exhibit agreement with the synthetic model, even at the intersection point.

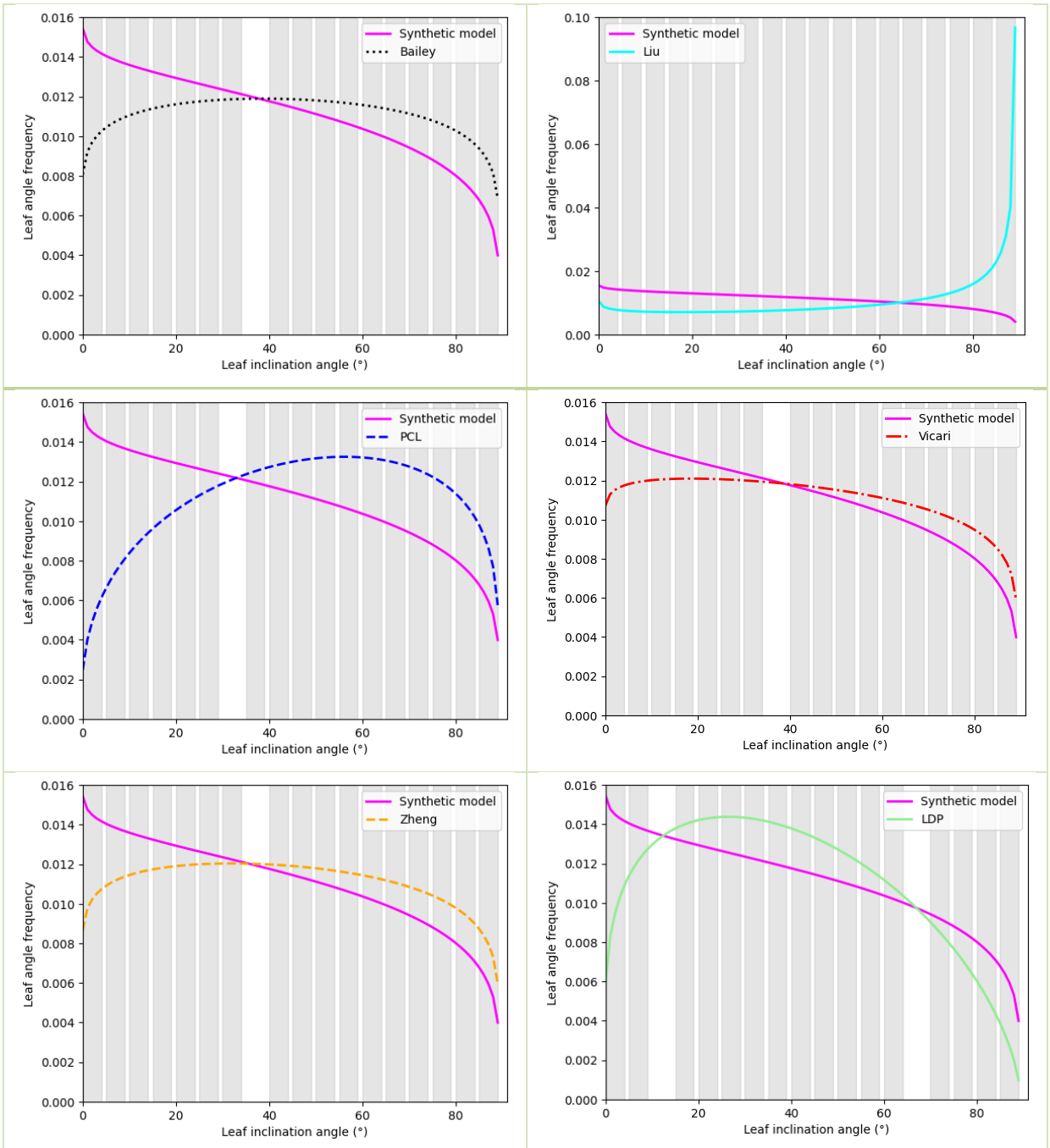

Figure 18: Comparative analysis results for the synthetic uniform TLS dataset at 5-degree intervals, with shaded regions indicating a statistically significant difference between the synthetic model and the LAD estimation method.

Table 14: Statistical results (The average leaf inclination angle (ALIA), standard deviation (SD), two parameters μ, ν, LAD type (Distribution) based on De Wit (1965), and the number of leaf normal replicates (NR)) from the LAD estimation approaches based on a simulated, uniform LAD, tree representation.

Algorithm	***ALIA***	***SD***	***μ***	***ν***	***Distribution***	***NR***
Synthetic model	39.72	25.03	1.22	0.97	uniform	14296
Bailey	44.45	25.03	1.13	1.1	uniform	411778
Liu	57.29	28.11	0.5	0.87	extremophile	959829
PCL	47.78	23.62	1.23	1.39	uniform	959947
Vicari	42.75	25.17	1.15	1.04	uniform	882231
Zheng	43.65	24.93	1.16	1.09	uniform	959949
LDP	39.56	22.69	1.61	1.26	uniform	229

4.3.3. Erectophile Synthetic Data LAD

The statistical results obtained from the LAD estimation approaches based on a simulated erectophile LAD tree representation are presented in Table 15. The synthetic model, representing an erectophile LAD, had an ALIA value of 66.38° and a standard deviation of 16.64°. All the TLS approaches were in relatively close agreement with the synthetic model's values, with the standard deviations also within a reasonable range of the synthetic model's values. Notably, the LDP algorithm yielded a slightly lower ALIA value of 64.8° compared to the other algorithms and the synthetic model. The LAD type was classified as erectophile for all methods. The PDFs of the various LAD estimation approaches, alongside the erectophile synthetic model, are presented in Figure 20. The methods depict an overall agreement with the synthetic model's PDF.

Table 15: Statistical results (The average leaf inclination angle (ALIA), standard deviation (SD), two parameters μ, ν, LAD type (Distribution) based on De Wit (1965), and the number of leaf normal replicates (NR)) from the LAD estimation approaches based on a simulated, erectophile LAD, tree representation.

Algorithm	***ALIA***	***SD***	***M***	***ν***	***Distribution***	***NR***
Synthetic model	66.38	16.64	1.22	3.44	erectophile	1351
Bailey	67.25	16.66	1.14	3.37	erectophile	177666
Liu	66.1	18.7	0.93	2.58	erectophile	306037
PCL	67.25	16.36	1.19	3.52	erectophile	306091
Vicari	67.33	16.21	1.21	3.6	erectophile	304876
Zheng	67.32	16.23	1.21	3.59	erectophile	306091
LDP	64.8	17.96	1.14	2.92	erectophile	205

Table 13 also displays the p-values obtained from the non-parametric Mann-Whitney U-test. The results show that all the algorithms, including the LDP approach, have p-values greater than 0.05. These results thus indicate no statistically significant difference between the estimates provided by these algorithms and the synthetic erectophile LAD tree representation at the chosen significance level. Additionally, the p-values obtained in this case suggest that the estimates obtained by these algorithms are in good agreement with the characteristics of the synthetic erectophile LAD model.

The comparative analysis between the erectophile LAD synthetic model and each LAD estimation method at 5-degree intervals is illustrated in Figure 19. The findings indicate that Bailey, PCL, Vicari, and Zheng consistently aligned with the synthetic model, except for the 80º-85º shaded interval, where significant differences were observed. On the other hand, the LDP and Liu methods demonstrated some

level of agreement with the synthetic model but within different angle intervals. The LDP method displayed agreement predominantly within the 45°-65° interval, while the Liu method showed agreement within the 35°-50° interval.

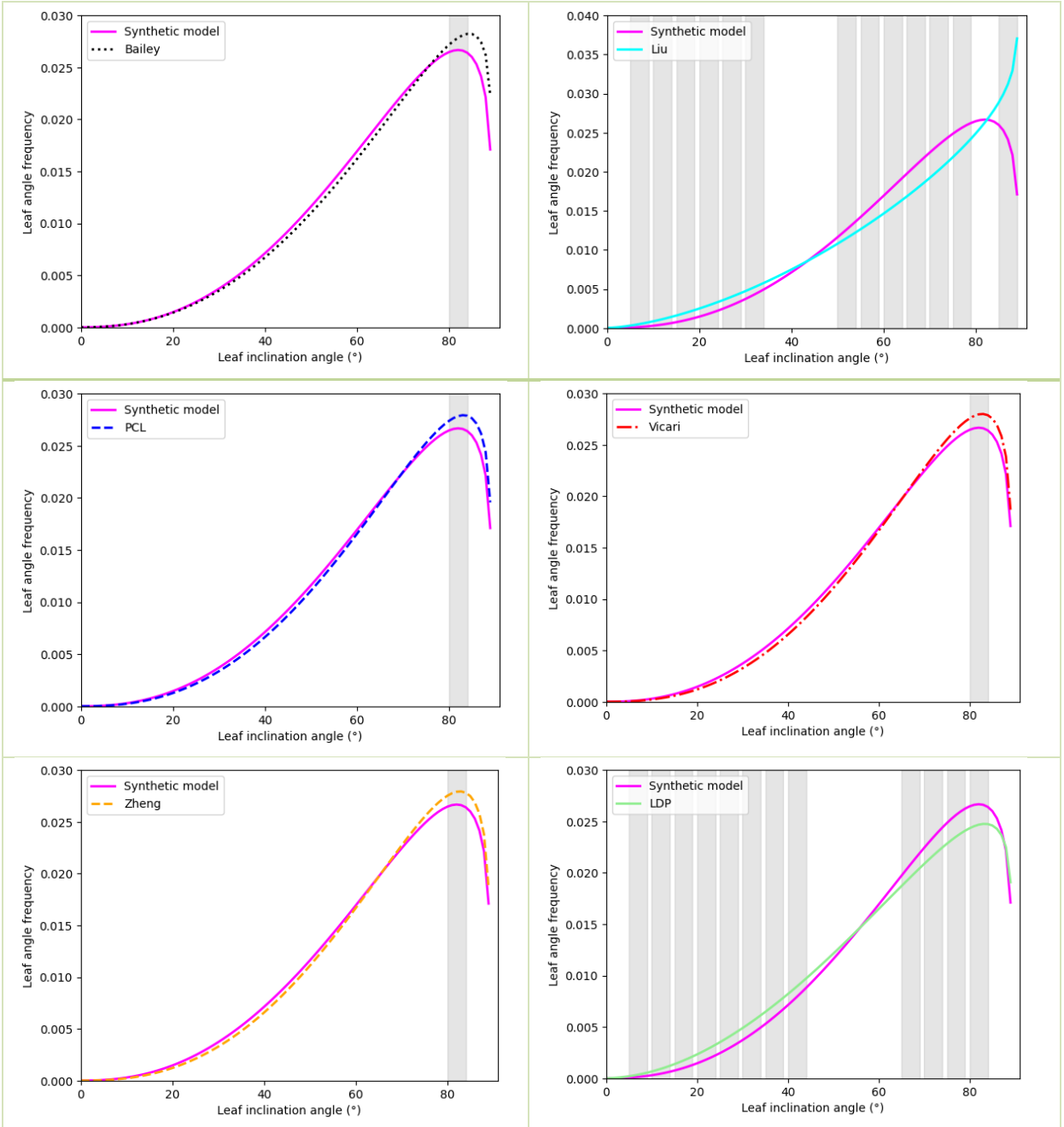

Figure 19: Comparative analysis results for the synthetic erectophile TLS dataset at 5-degree intervals, with shaded regions indicating a statistically significant difference between the synthetic model and the LAD estimation method.

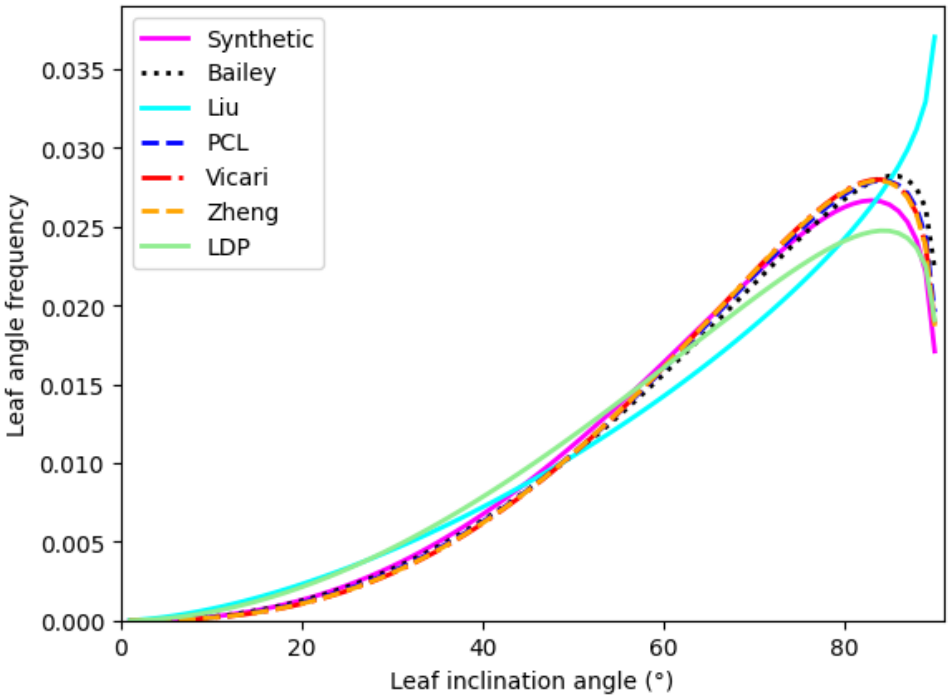

Figure 20: Fitted beta distributions of LIAs for the simulated erectophile LAD tree representation.

5. DISCUSSION

5.1. LAD Estimation from Real Trees

The autumn season conditions at Kumpula Gardens (Helsinki, Finland) may have influenced the leaf orientation, as evidenced by the yellowing and drooping of leaves (Figures 6, 7, 8, 9 (a)), indicating the onset of senescence. The algorithms used in this study consistently predicted prevalent spherical and erectophile LAD types as expected (Tables 2, 3, 4, 5). Among the species studied from the Kumpula Garden, *Fagus sylvatica* demonstrated the best agreement between the TLS algorithms regarding the LAD type. The least agreement was for the *Pyrus comμnis 'Olga'*. The standard deviation was noted to be comparable in most cases. Although the LAD estimations by the Liu algorithm were generally consistent with other approaches, the algorithm showed a consistently biased pattern in its PDFs, as shown in Figures 6, 7, 8, 9 (b), with a bias towards leaf inclination angles close to 90º. Moreover, as noted by Darwin (1881), Ehleringer and Forseth (1980), and Muraoka et al. (1998), plants can adjust their leaf angles in response to environmental changes and for resource acquisition, mainly light. Figure 21 illustrates a *Rhododendron cf branchycarpum* shrub tree showing an upright or vertical leaf orientation, which is characteristic of the plant's growth during more favourable summer conditions. In contrast, the drooping leaves observed in the scanned *Rhododendron cf branchycarpum* shrub tree in this study (Figure 8(a)) indicate a shift towards a water conservation state, reflecting the colder autumn conditions experienced in Helsinki. Therefore, the spherical and erectophile LAD types for the tree shown by the TLS algorithms suggest a drooping state LAD type rather than the vertical state LAD type.

Figure 21: An image of a Rhododendron cf branchycarpum shrub tree showing an upright or vertical leaf orientation, characteristic of the plant's growth during more favourable summer conditions. Credit: Prof. Dr. A.K. Skidmore.

The LDP approach was generally consistent with the TLS approaches. However, the method remarkably indicated a different LAD type (plagiophile) for the European beech tree (*Fagus sylvatica)*. The LDP approach has limitations, particularly its reliance on structures like poles, windows of tall buildings, ladders, and towers to capture canopy photographs (Chianucci et al., 2018; Raabe et al., 2015). In this case, the ladder available during data collection was shorter than the tree; hence the whole tree was not covered. LAD can vary at different height levels within the canopy (Niinemets, 2010). The upper canopy levels

often exhibit steeper leaf angles, while the middle and bottom layers tend to have more horizontal and lateral growth directions (Niinemets, 2010). Thus, the LDP method may have undersampled the steeper angles (erectophile), leading to a lower proportion of these angles being represented by the approach. In contrast, TLS captures the entire height profile of a canopy (Moskal and Zheng, 2012), ensuring that the steeper leaves at the top are not missed. Therefore, TLS provides a more comprehensive representation of the canopy structure compared to the LDP approach, which relies on limited perspectives from the available platforms. To overcome this limitation, alternative methods, such as deploying unmanned aerial vehicles (UAVs), as demonstrated by McNeil et al. (2016), can provide a more complete assessment of the canopy structure and leaf angles and, if used as a platform for LDP can capture the entire canopy.

The analysis of trees from Kew Garden revealed a wider variety of LAD types compared to the Kumpula Gardens dataset. In addition to spherical and erectophile LAD types, uniform and plagiophile LAD types were observed (Tables 6 and 9). The TLS algorithms generally agreed on the LAD type estimations, except for cases where the Liu algorithm displayed a preference towards leaf inclination angles close to 90º. This biased pattern was evident in the LAD type estimation for the *Wollemia nobilis*, where the algorithm indicated a bias towards both the 0º and 90º edges, as shown in Figure 9(b). Notably, when the TLS algorithms classification returned either a spherical or plagiophile LAD type, the Liu algorithm exhibited a pattern consistent with the rest of the algorithms. This agreement suggests that the Liu algorithm performed well in cases where the LAD type was spherical or plagiophile but struggled to estimate other LAD types accurately. The TLSLeAF algorithm also returned a spherical LAD type consistently, indicating the LAD type in every instance for the two study areas. This preference suggests a possible limitation and suitability of the TLSLeAF algorithm in capturing the full range of different LAD types. Additionally, the scanned images of *Ginkgo biloba* and *Ostrya japonica* (Figure 11(a) and 12(a), respectively) exhibited signs of drooping leaves. Therefore, the spherical and erectophile LAD types suggested by the algorithms for these species indicate a state of water conservation rather than simply reflecting leaf orientation under favourable conditions, as also seen with the *Rhododendron cf branchycarpum*. This interpretation is influenced by the timing of the data collection exercise (autumn) and the specific characteristics of the scanned trees.

Similar to the Kumpula dataset, the LDP approach demonstrated consistent results with TLS algorithms for the Kew Gardens. However, the approach showed significantly different ALIA and standard deviation values compared to the TLS algorithms in the case of the *Diospyros lotus*. This discrepancy could be attributed to the curvature exhibited by the leaves of this species, as the LDP approach is tailored for species with flat leaves (Pisek et al., 2011; Chianucci et al., 2018). On the other hand, TLS approaches are not limited by leaf curvature. Depending on the footprint of the TLS on the target, TLS can retrieve LAD information from more complex leaf surfaces (Vicari et al., 2019). Therefore, TLS provides a more thorough method for analysing leaf angles, particularly in cases where leaf curvature is present.

The TLS algorithms demonstrated a high number of replicates for estimating leaf normals, benefiting from the high sampling resolutions provided by TLS scans to capture detailed information about leaf surfaces. For instance, the Bailey algorithm utilises the point clouds to create a mesh of triangles along leaf surfaces that facilitates the calculation of normal vectors at the position of each triangle (Bailey and Mahaffee, 2017). TLSLeAF leverages gridded point clouds at the pixel level to estimate multiple angles for each leaf, thus accommodating the diverse structure and curvature of leaves (Stovall et al., 2021). The Vicari algorithm obtains LAD information by fitting all applicable planes to leaf point clouds (Vicari et al., 2019). On the other hand, the LDP approach performs optimally with flat leaves, as evidenced by its agreement with the TLS methods in the case of *Wollemia nobilis* (Figure 10(a)), where the leaves had minimal curvature. However, the scanned *Diospyros lotus* tree (Figure 13(a)) exhibited leaves with varying

degrees of curvature, which likely contributed to the significant differences observed in the ALIA and PDFs between the LDP method and the TLS algorithms (Figure 13(b) and Table 9).

5.2. Statistical Analysis

In this study, the inter-comparison of algorithm pairs for both the Kumpula and Kew datasets provided insight into their level of agreement and discrepancies (Tables 10 and 11). The Mann-Whitney U-test was employed to assess the significance of these differences, shedding light on the robustness and reliability of the algorithms.

For the Kumpula dataset, the analysis revealed a generally high level of agreement among the algorithms, as indicated in Table 10. Specifically, a more significant agreement was observed for the *Rhodendron cf brachycarpum* and *Fagus sylvatica* species. However, there were instances of disagreement among the algorithms, particularly in the case of the *Pyrus communis 'Olga'*. Notably, the Liu algorithm demonstrated the highest level of agreement with the Zheng algorithm, with no significant difference across the four species tested. On the contrary, the TLSLeAF and Bailey algorithms did not align with the Liu algorithm's PDFs for any of the four species. The LDP approach exhibited consistency with the TLS algorithms, except for disagreements with the Bailey and TLSLeAF algorithms regarding the *Pyrus communis 'Olga'*.

There were no significant differences between the TLS algorithms for all species of the Kew dataset, except for the *Wollemia nobilis*, where the Liu algorithm showed a significant difference compared to all the other algorithms, as shown in Table 11. There was a remarkable 100% agreement among all algorithms for the *Diospyros lotus* species, highlighting the proficiency of the Liu algorithm in cases where the LAD type was either spherical or plagiophile. The LDP approach demonstrated a significant agreement with the TLS algorithms for the *Wollemia nobilis* and *Ginkgo biloba* tree species, except for the *Wollemia nobilis* with the Liu algorithm. However, the LDP approach showed more disagreements and marginal agreements with the TLS algorithms in the *Ostrya japonica* and *Diospyros lotus* cases. This discrepancy could be attributed to the curvature present in the leaves of these species, which better suit the TLS approaches but pose limitations on the effectiveness of the LDP method (Vicari et al., 2019).

The high level of agreement observed among the algorithms for most species in both datasets is encouraging, indicating their consistency and reliability. However, disagreements and discrepancies in some instances highlight the need for further investigation and improvement.

5.3. LAD Estimation from Simulated Tree Representations

The assessment and comparison of various LAD estimation approaches using simulated tree representations of different LAD types (spherical, uniform, and erectophile) provided a further evaluation of the performance and agreement of the approaches with the corresponding synthetic models. Most of the techniques demonstrated comparable estimates of the ALIA, SD (Table 12), and PDFs (Figure 15) within an acceptable range of the synthetic model's output for the simulated spherical LAD tree representation. This finding suggests that these approaches effectively captured the spherical LAD characteristics. The statistical analysis further supported this conclusion, with the tests indicating no statistically significant difference between the algorithms and the synthetic model (p-value > 0.05) (Table 13). However, the Liu algorithm showed the least (but still significant) agreement, also indicated by its higher ALIA value.

In contrast, the synthetic uniform LAD tree representation presented a wider range of ALIA values by the LAD estimation methods compared to the spherical model (Table 14). Notably, the Liu algorithm exhibited a significantly different ALIA value and LAD type compared to the others, indicating a

departure from the expected uniform LAD pattern. The statistical analysis confirmed this significant difference by the Liu algorithm (Table 13). On the other hand, the other algorithms displayed no significant difference from the synthetic uniform model, demonstrating reasonable agreement in estimating this LAD type.

The p-value results (Table 13) of the synthetic erectophile LAD tree representation revealed that all the evaluated LAD estimation approaches exhibited no statistically significant difference from the synthetic model. This agreement suggests that the algorithms provided estimates that aligned well with the characteristics of the erectophile LAD model, with the model characterised by steeper leaf angles; hence higher ALIA values were expected.

The comparative analyses at 5-degree intervals conducted between the synthetic LAD models and each LAD estimation method facilitated further evaluation of the performance and accuracy of these methods across different angle intervals. In the analysis with the spherical LAD synthetic model, algorithms exhibited statistically significant differences in specific angle ranges, indicating deviations from the model (Figure 16). The Liu approach consistently displayed significant differences throughout, suggesting potential limitations in accurately estimating the LAD. The LDP method also showed significant differences at various intervals, likely due to its estimation of LAD from a subset of leaves rather than considering the entire canopy, which is a distinguishing factor from the TLS methods. The analysis with the uniform synthetic model revealed significant differences between the LAD estimation methods and the model (Figure 18), suggesting a more limited capability of the methods in accurately estimating more horizontally-aligned LADs. In the analysis with the erectophile LAD synthetic model, all algorithms consistently aligned with the model, with some significant differences observed in specific angle intervals. However, the algorithms showed agreement with the model over most of the LAD range. The significant difference between the erectophile model and most of the algorithms only at the 80º-85º interval could probably be due to the occlusion of part of the model from the view of the scanner.

The findings from the different simulated tree representations indicate the varying performance of the LAD estimation approaches. Most algorithms showed no significant differences with the synthetic models for spherical and erectophile LAD types. However, challenges were encountered when dealing with the uniform LAD type, particularly with the Liu algorithm. According to Bailey and Mahaffee (2017), their triangulation method performs best when LADs have more leaf area projected towards the scanner. This observation could explain why the spherical and erectophile LADs showed better agreement than the uniform model, as they have more leaf area facing the scanner's direction. The comparative analysis at 5-degree intervals further supports these findings by highlighting the varying performance of the algorithms in estimating LAD.

5.4. LAD Estimation Methods Strengths and Weaknesses

The LAD estimation approaches used in this study demonstrated both strengths and weaknesses. These strengths and weaknesses were assessed based on various aspects, including setup, input data formats, LAD estimation procedures, and overall performance in the conducted tests. This section aims to provide an overview of the strengths and limitations associated with each LAD estimation approach.

The Bailey algorithm involves a relatively complex setup procedure; however, its detailed documentation and available tutorials greatly facilitated the process. The method does not account for differentiating between wood and leaves (Bailey and Mahaffee, 2017). It compensates for the bias introduced by the scanner position in estimating leaf angles (Bailey and Mahaffee, 2017). This compensation is achieved through separate scans for each scan position, saved in an ASCII file format, and an accompanying XML

file specifying scan parameters (such as scanner position, resolution, intensity, etc.) (Figure 5). The algorithm's performance with the Kumpula Garden data raised concerns regarding its ability to differentiate between spherical and erectophile LADs, as it consistently indicated spherical LADs for all four trees. However, these concerns were alleviated by the results obtained from the Kew Garden and simulated datasets, where the algorithm successfully predicted LAD types other than spherical. Bailey and Mahaffee (2017) mention that the algorithm was found to be minimally impacted by variations in scan resolution. It is possible that the small observed discrepancies could be influenced by the relatively low-density areas of the single low-resolution scans used with the algorithm. Overall, the algorithm demonstrated consistency in agreement with other TLS approaches. The comparative analysis conducted at 5-degree intervals using high-resolution synthetic point clouds highlighted the method's superior performance with erectophile LAD types and its relatively lower performance with the uniform LAD type. This discrepancy in performance can be attributed to the amount of leaf area projected towards the scanner. However, the algorithm is expected to address this issue by applying weighting to triangles, mitigating bias towards normal vectors that face the TLS scanner (Bailey and Mahaffee, 2017).

The Liu algorithm stands out for its relatively simple setup process, requiring the establishment of a Python 3 environment and specifying the leaf constraint and input point cloud location. The input point cloud for each tree follows the widely used ASCII format (Pepe et al., 2016). In contrast to the Bailey approach, the Liu algorithm requires an extra step since it generates LAD information by using point clouds generated from merging co-registered individual scans to increase point density (Liu et al., 2019). While the method recognises the importance of differentiating leaves from woody material, it does not possess this feature by default. The original study employed a Support Vector Machine (SVM) classification technique to separate leaves from wood. The algorithm's consistency with the ALIA values of other TLS algorithms is notable. However, it exhibited poor performance when fitting the beta distribution, with distinct differences in patterns compared to the other algorithms. This discrepancy may indicate an underlying flaw in the algorithm's execution, as reflected by its estimated ALIA or SD values, which tended to be higher than those of other algorithms in most cases. Regarding LAD prediction with synthetic models, the Liu algorithm still managed to identify the synthetic spherical LAD type, although some erroneous patterns were evident. Conversely, it encountered challenges in predicting the uniform LAD model. The Liu algorithm generally performed well in identifying the synthetic erectophile model, as the comparative analysis conducted at 5-degree intervals revealed.

The PCL algorithm requires a complex setup process, even when using its prebuilt binaries designed for different operating systems. In this study, a Linux environment was chosen to execute the algorithm. The algorithm relies on merged ASCII point clouds, which serve as the precursor to the Point Cloud Data (PCD) format, the designated input data format for PCL. The PCL algorithm exhibited exceptional performance, consistently aligning with the outcomes of other TLS algorithms. Its impressive performance in the comparative analysis conducted at 5-degree intervals was particularly noteworthy, specifically when estimating the synthetic spherical model LAD. The algorithm demonstrated strong agreement with the leaf orientation of the model, with no significant disagreements observed at any interval. Moreover, its predictions of the synthetic model's LAD type displayed excellent performance, with only one interval showing a significant difference. Overall, the PCL algorithm showcased robust and reliable performance, consistently producing results that aligned closely with other TLS algorithms.

TLSLeAF is an accessible and user-friendly open-source algorithm that can be easily set up by cloning its R source code from the associated GitHub account and ensuring the installation of the required dependency, a point cloud processing software (Cloud Compare). However, the algorithm's gridded input data format differs from the widely used ASCII file formats. Converting existing ASCII files into the PTX

or similar gridded data formats can be challenging. The PTX format, on the other hand, offers valuable individual scan information such as point cloud size, transformation parameters, scanner position, intensity, and more. Similar to the Bailey algorithm, the PTX format allows for the consideration of scanner position bias in estimating LAD without requiring a separate file for scan metadata. TLSLeAF distinguishes itself from other algorithms by offering an inherent feature for separating leaves from wood (Stovall et al., 2021). This additional capability gives TLSLeAF a theoretical advantage, eliminating the need for external methods or techniques to differentiate between these components. It shall be noted that this study did not evaluate the performance of this leaf-wood separation feature. In terms of performance, TLSLeAF generally displayed consistency with other TLS algorithms. However, a notable limitation arose in its ability to accurately predict LAD types other than spherical, where it performed poorly. This raises questions about the algorithm's effectiveness in estimating non-spherical LAD types. Despite this limitation, TLSLeAF remains an accessible and convenient algorithm for LAD estimation, with a straightforward setup process. However, further exploration and improvement is recommended and may be needed to enhance its capability to predict a wider range of LAD types.

The setup process for the Python 2-based Vicari algorithms can be relatively complex in regard to linking modules and obtaining the necessary dependencies. However, like the Liu and PCL algorithms, Vicari utilises merged ASCII format point clouds as input data. The results obtained from the Vicari algorithm demonstrated consistency with other TLS approaches, closely aligning with the performance of both the PCL and Zheng algorithms in most cases. Using simulated datasets further highlighted the algorithm's strong performance, with only the PCL algorithm expressing a better agreement with the synthetic spherical LAD model in the comparative analysis at 5-degree intervals (Figure 16). Additionally, the Vicari algorithm showcased impressive performance in the comparative analysis of the synthetic erectophile model, ranking among the four algorithms that exhibited the highest agreement with the model. Despite its somewhat complicated setup process, the Vicari algorithm proved reliable and effective for LAD estimation.

The setup process for the Zheng algorithm is challenging. It requires older versions of dependencies such as Visual Studio 2015 update 3, boost 1.60.0, Eigen3, and CGAL 4.11.1, which may pose challenges when integrating them into the latest computing environments. Similar to the Liu, PCL, and Vicari algorithms, the Zheng algorithm uses co-registered and merged point clouds in the widely used ASCII format for LAD estimation. It does not include a feature for leaf-wood separation. Despite the intricate setup process, the Zheng algorithm demonstrates consistency with other TLS algorithms. Notably, it exhibits similar patterns to both the PCL and Vicari algorithms. In the comparative analysis conducted at 5-degree intervals, the algorithm's strong performance becomes evident, displaying a high level of agreement with both the spherical and erectophile LAD types. However, like other algorithms, it encountered challenges when estimating the simulated, synthetic uniform LAD type.

The LDP method is limited due to its manual, non-automated selection of appropriate leaves for LAD estimation, as Vicari et al. (2019) noted. However, this method offers the advantage of strictly utilising photosynthetic material exclusively for LAD estimation through manual leaf-by-leaf assessment. Another drawback of the LDP method is its limited accuracy in estimating LAD for curved leaves, unlike the TLS algorithms. This limitation became particularly evident in the LAD estimation of curved *Diospyros lotus* leaves (Figure 13). Despite these limitations, the LDP approach exhibited general consistency and compatibility with the TLS algorithms, mainly when the leaves exhibited minimal curvature. Although the TLS algorithms demonstrated superior LAD estimations when a more significant proportion of leaf area was projected towards the scanner, closer to the synthetic spherical and erectophile models, the LDP approach demonstrated proficiency in estimating the synthetic uniform model. It obtained an ALIA value

closest to the model, showcasing its competence in cases where leaf distribution is more horizontal and exhibits less curvature. This observation was further supported by the agreement between the LDP approach and the TLS algorithms in the case of the *Wollemia nobilis* (Figure 10).

As scan density increases, the errors in estimating the LAD decrease (Bailey and Mahaffee, 2017). Some single scans may exhibit a lower density of points, impacting the quality of LAD estimation. Most methods in this study overcome this limitation by using merged scans to increase the overall point density. TLSLeAF addresses density measurement bias by calculating statistics of angle measurements within voxels and reconstructing the distribution of measurements using an equal number of simulated angles (Stovall et al., 2021). Despite such measures, algorithms that utilise merged point clouds performed better than their single-scan counterparts in this study. This finding suggests the benefits of merging multiple scans to increase point density and enhance LAD estimation accuracy could outweigh the concern for the bias introduced by the scanner position in estimating leaf angles. This performance disparity emphasises the need for further investigation into the choice of using either single or combined scans for LAD estimation.

The TLS algorithms demonstrated varying processing speeds depending on the time required to estimate the LAD. While the speeds differed among the algorithms, they exhibited consistent processing speeds across all point clouds that were analysed. As an example, the processing times for the *Rhododendron cf brachycarpum* point cloud, made of 3,753,702 data points from four scan positions, were achieved (Table 12). The reported processing speeds in Table 12 correspond to the calculations done on the Lenovo Thinkpad P15s Gen 1 laptop with a Core i7 CPU (full specifications in Section 3.3). TLSLeAF exhibited the fastest processing speeds for LAD estimation, processing each individual point cloud separately before the overall LAD was obtained. This performance confirms its rapid processing robustness, as Stovall et al. (2021) outlined. The Bailey, Vicari, and PCL methods followed, respectively, where each algorithm efficiently estimated the LAD while maintaining reasonable processing times. The Liu algorithm required close to 44 minutes to fully process the data, indicating a relatively longer processing duration. The Zheng algorithm exhibited the longest processing duration. However, it compensates for this longer duration with its relatively good performance in LAD estimation observed in this study.

Table 12: Ranking of TLS algorithms based on their processing durations for the Rhododendron cf brachycarpum point cloud.

Algorithm	***Processing speed***
TLSLeAF	1 minute 56 seconds
Bailey	3 minutes 35 seconds (normals estimation)
Vicari	4 minutes 32 seconds
PCL	4 minutes 43 seconds (normals estimation)
Liu	43 minutes 42 seconds
Zheng	1 hour 38 minutes (normals estimation)

5.5. Study Challenges

The study illustrated how well the various LAD estimation approaches performed against each other. However, some challenges may have influenced the inter-comparison outcomes. These challenges include:

5.5.1. Leaf-wood Separation

A common tool was employed, with most methods lacking a built-in leaf-wood separation feature. As a result, the Liu, PCL, Vicari, and Zheng algorithms were tested using the same leaf-only point clouds. Similarly, the Bailey algorithm was tested with leaf-only point clouds but as individual scans. However, due

to the TLSLeAF algorithm possessing its leaf-wood separation capability, its input consisted of the full, unseparated versions of the trees' point clouds. This discrepancy in leaf-wood separation between TLSLeAF and the other algorithms introduces a potential source of inconsistency in the inter-comparison of LAD estimation methods, which may have compromised the accuracy of the evaluation. Leaf-wood separation methods themselves may have encountered challenges in accurately classifying leaves from wood. However, the utilisation of synthetic scans helped mitigate such discrepancies, as the meshes used to create the models were well-defined and known.

5.5.2. Input Data File Formats

TLS algorithms commonly (five out of 6 in this study) use the ASCII file format. However, TLSLeAF employs the PTX file format or other gridded file formats. While the PTX format offers a higher level of scan information compared to a plain ASCII point cloud, it is not as widely adopted. The study encountered difficulties in generating PTX data successfully, which restricted the inclusion of TLSLeAF in the analysis (Section 4.3). The choice of file format in TLS algorithms depends on various factors such as data requirements, compatibility with software tools, and specific project needs. While the ASCII format is commonly used, alternative formats like PTX may be preferred in some instances that demand more detailed scan information or specialised processing.

5.5.3. Scanner Resolution

Bailey and Mahaffee (2017) reported that their algorithm demonstrated minimal sensitivity to variations in scan resolution. Additionally, Stovall et al. (2021) emphasized that lower scan resolutions could enhance the variation in LAD while closely approximating the true LAD on average. In this study, the real scans obtained from the botanical gardens generally had relatively lower resolutions, whereas the simulated scans had high resolutions. Since the same scans were used across all the algorithms, it is not expected that the scan resolution would have influenced the inter-comparison of the algorithms here.

5.5.4. Occlusion

One inherent limitation of LiDAR and other optical approaches is occlusion, which occurs when leaves are entirely obstructed from the view of the laser, resulting in their exclusion from the measurements. Occlusion can be a source of measurement error (Stovall et al., 2021). Consequently, the estimated LADs may exhibit a bias towards leaves that are not occluded from the scanner's view (Bailey and Mahaffee, 2017). Multiple scanner positions can be employed to mitigate this issue to some extent, as demonstrated in this study's scanning of synthetic models, where eight scanner positions were set for each model. Despite these precautions, occlusion-related challenges may persist, as evidenced in this study. While most algorithms exhibited agreement with the synthetic erectophile model's characteristics across various angles, none of them could satisfactorily match the model's features within the 80º-85º interval (Figure 19). This observation suggests the presence of unmeasured sections within the 3D model, further emphasizing the impact of possible occlusion on LAD estimation accuracy.

6. CONCLUSION AND RECOMMENDATIONS

6.1. Conclusion

This study tested, compared, and evaluated the performance of six TLS LAD estimation methods using LiDAR data from real trees and synthetic 3D model trees. Furthermore, there was a comparison between the performance of these TLS-based algorithms with the established LDP approach. Based on the study's research questions, the following conclusion was drawn:

- Agreement among independent methods in retrieving LAD information from LiDAR data: Analysis of real trees from the Kumpula and Kew Gardens' datasets revealed a high level of agreement among the TLS algorithms, indicating their general consistency and reliability. Nonetheless, the Liu and the TLSLeAF algorithms displayed preferences towards specific LAD types, suggesting possible limitations in capturing the full range of different LAD types. These findings emphasize the importance of considering algorithm suitability and limitations in practical applications.

- Each LAD estimation approach demonstrated both strengths as well as limitations. The Bailey algorithm, despite its complex setup process, compensated for scanner position bias and exhibited good consistency with other TLS approaches. With its relatively simple setup process, the Liu algorithm showed discrepancies in its estimated ALIA values and patterns. Although the PCL algorithm required a complex setup process, it demonstrated exceptional performance and strong agreement with other TLS algorithms. The LDP approach consistently produced results comparable to the TLS algorithms but had limitations in securing access to upper parts of canopies and in accurately estimating LAD where there was complex leaf curvature. The TLS-based methods provided a more comprehensive representation of the canopy structure, capturing the entire height profile and overcoming the limitations of the LDP approach.

6.2. Recommendations for Future Research

Based on the findings of this study, the following recommendations can be made:

- Further research is necessary to explore the impact of using single or combined scans on LAD estimation.
- More attention should be directed towards developing efficient and practical techniques for initial leaf-wood separation of TLS data to improve LAD estimation accuracy.
- This study may serve as a template for establishing benchmark datasets, evaluation protocols, and accessibility of algorithms that could facilitate systematic comparisons of LAD estimation algorithms, similar to the Radiation transfer Model Intercomparison (RAMI) exercise (Widlowski et al., 2015). This collaborative effort could promote fairness, reproducibility, and the advancement of LAD estimation techniques by enabling researchers to identify strengths, weaknesses, and areas for improvement in their algorithms.

LIST OF REFERENCES

Asner, G. P. (1998). Biophysical and biochemical sources of variability in canopy reflectance. *Remote Sensing of Environment*, *64*(3), 234–253.

Aspose.3D Product Family. (n.d.). Retrieved 11 April 2023, from https://docs.aspose.com/3d/

Bailey, B. N., & Mahaffee, W. F. (2017). Rapid, high-resolution measurement of leaf area and leaf orientation using terrestrial LiDAR scanning data. *Measurement Science and Technology*, *28*(6), 064006. https://doi.org/10.1088/1361-6501/aa5cfd

Bayer, D., Seifert, S., & Pretzsch, H. (2013). Structural crown properties of Norway spruce (Picea abies [L.] Karst.) and European beech (Fagus sylvatica [L.]) in mixed versus pure stands revealed by terrestrial laser scanning. *Trees*, *27*(4), 1035–1047.

canopy—SCOPE 1.8 documentation. (n.d.). Retrieved 9 June 2023, from https://scope-model.readthedocs.io/en/2.1/structs/input/canopy.html

Chen, J. M., & Black, T. A. (1992). Defining leaf area index for non-flat leaves. *Plant, Cell & Environment*, *15*(4), 421–429.

Chen, J. M., Black, T. A., & Adams, R. S. (1991). Evaluation of hemispherical photography for determining plant area index and geometry of a forest stand. *Agricultural and Forest Meteorology*, *56*(1–2), 129–143.

Chen, J. M., & Cihlar, J. (1996). Retrieving leaf area index of boreal conifer forests using Landsat TM images. *Remote Sensing of Environment*, *55*(2), 153–162. https://doi.org/10.1016/0034-4257(95)00195-6

Chianucci, F., Pisek, J., Raabe, K., Marchino, L., Ferrara, C., & Corona, P. (2018). A dataset of leaf inclination angles for temperate and boreal broadleaf woody species. *Annals of Forest Science*, *75*(2), Article 2. https://doi.org/10.1007/s13595-018-0730-x

Cifuentes, R., Van der Zande, D., Farifteh, J., Salas, C., & Coppin, P. (2014). Effects of voxel size and sampling setup on the estimation of forest canopy gap fraction from terrestrial laser scanning data. *Agricultural and Forest Meteorology*, *194*, 230–240. https://doi.org/10.1016/j.agrformet.2014.04.013

Colaizzi, P. D., Evett, S. R., Brauer, D. K., Howell, T. A., Tolk, J. A., & Copeland, K. S. (2017). Allometric Method to Estimate Leaf Area Index for Row Crops. *Agronomy Journal*, *109*(3), 883–894. https://doi.org/10.2134/agronj2016.11.0665

Darwin, C. (1881). Movements of plants. *Nature*, *23*(592), 409–409.

Daughtry, C. S. T. (1990). Direct measurements of canopy structure. *Remote Sensing Reviews*, *5*(1), 45–60. https://doi.org/10.1080/02757259009532121

Demol, M., Verbeeck, H., Gielen, B., Armston, J., Burt, A., Disney, M., Duncanson, L., Hackenberg, J., Kükenbrink, D., Lau, A., Ploton, P., Sewdien, A., Stovall, A., Takoudjou, S. M., Volkova, L., Weston, C., Wortel, V., & Calders, K. (2022). Estimating forest above-ground biomass with terrestrial laser scanning: Current status and future directions. *Methods in Ecology and Evolution*, *13*(8), 1628–1639. https://doi.org/10.1111/2041-210X.13906

EC. (2020). *EU Biodiversity Strategy for 2030. Bringing nature back into our lives.*

Ehleringer, J., & Forseth, I. (1980). Solar tracking by plants. *Science*, *210*(4474), 1094–1098.

Factsheet: EU 2030 Biodiversity Strategy. (n.d.). [Text]. European Commission - European Commission. Retrieved 5 January 2023, from https://ec.europa.eu/commission/presscorner/detail/en/fs_20_906

Foundation, B. (n.d.). Blender.org—Home of the Blender project—Free and Open 3D Creation Software. *Blender.Org*. Retrieved 28 April 2023, from https://www.blender.org/

Fournier, R., & Hall, R. J. (2017). *Hemispherical Photography in Forest Science: Conclusions, Applications, Limitations, and Implementation Perspectives*. https://doi.org/10.1007/978-94-024-1098-3_10

García-Haro, F. J., Campos-Taberner, M., Muñoz-Marí, J., Laparra, V., Camacho, F., Sánchez-Zapero, J., & Camps-Valls, G. (2018). Derivation of global vegetation biophysical parameters from EUMETSAT Polar System. *ISPRS Journal of Photogrammetry and Remote Sensing*, *139*, 57–74. https://doi.org/10.1016/j.isprsjprs.2018.03.005

Geijzendorffer, I. R., Regan, E. C., Pereira, H. M., Brotons, L., Brummitt, N., Gavish, Y., Haase, P., Martin, C. S., Mihoub, J.-B., & Secades, C. (2016). Bridging the gap between biodiversity data and policy reporting needs: An Essential Biodiversity Variables perspective. *Journal of Applied Ecology*, *53*(5), 1341–1350.

Goel, N. S., & Strebel, D. E. (1984). Simple beta distribution representation of leaf orientation in vegetation canopies 1. *Agronomy Journal*, *76*(5), 800–802.

Gonsamo, A., & Pellikka, P. (2009). The computation of foliage clumping index using hemispherical photography. *Agricultural and Forest Meteorology*, *149*(10), 1781–1787. https://doi.org/10.1016/j.agrformet.2009.06.001

Gonzalez de Tanago, J., Lau, A., Bartholomeus, H., Herold, M., Avitabile, V., Raumonen, P., Martius, C., Goodman, R. C., Disney, M., & Manuri, S. (2018). Estimation of above-ground biomass of large tropical trees with terrestrial LiDAR. *Methods in Ecology and Evolution*, *9*(2), 223–234.

Goudriaan, J. (1988). The bare bones of leaf-angle distribution in radiation models for canopy photosynthesis and energy exchange. *Agricultural and Forest Meteorology*, *43*(2), 155–169. https://doi.org/10.1016/0168-1923(88)90089-5

Gratani, L., & Ghia, E. (2002). Changes in morphological and physiological traits during leaf expansion of Arbutus unedo. *Environmental and Experimental Botany*, *48*(1), 51–60. https://doi.org/10.1016/S0098-8472(02)00010-2

Gutschick, V. P. (1991). Joining leaf photosynthesis models and canopy photon-transport models. In *Photon-Vegetation Interactions* (pp. 501–535). Springer.

Helios Documentation v1.2.58. (n.d.). Retrieved 28 April 2023, from https://baileylab.ucdavis.edu/software/helios/

Homem Antunes, M. A., Walter-Shea, E. A., & Mesarch, M. A. (2001). Test of an extended mathematical approach to calculate maize leaf area index and leaf angle distribution. *Agricultural and Forest Meteorology*, *108*(1), 45–53. https://doi.org/10.1016/S0168-1923(01)00219-2

Hosoi, F., & Omasa, K. (2006). Voxel-Based 3-D Modeling of Individual Trees for Estimating Leaf Area Density Using High-Resolution Portable Scanning Lidar. *IEEE Transactions on Geoscience and Remote Sensing*, *44*(12), 3610–3618. https://doi.org/10.1109/TGRS.2006.881743

Hosoi, F., & Omasa, K. (2015). Estimating leaf inclination angle distribution of broad-leaved trees in each part of the canopies by a high-resolution portable scanning lidar. *Journal of Agricultural Meteorology*, *71*(2), 136–141. https://doi.org/10.2480/agrmet.D-14-00049

Hu, R., Bournez, E., Cheng, S., Jiang, H., Nerry, F., Landes, T., Saudreau, M., Kastendeuch, P., Najjar, G., Colin, J., & Yan, G. (2018). Estimating the leaf area of an individual tree in urban areas using terrestrial laser scanner and path length distribution model. *ISPRS Journal of Photogrammetry and Remote Sensing*, *144*, 357–368. https://doi.org/10.1016/j.isprsjprs.2018.07.015

Itakura, K., & Hosoi, F. (2019). Estimation of Leaf Inclination Angle in Three-Dimensional Plant Images Obtained from Lidar. *Remote Sensing*, *11*(3), 344. https://doi.org/10.3390/rs11030344

Jin, S., Tamura, M., & Susaki, J. (2016). A new approach to retrieve leaf normal distribution using terrestrial laser scanners. *Journal of Forestry Research*, *27*(3), 631–638. https://doi.org/10.1007/s11676-015-0204-z

Jonckheere, I., Fleck, S., Nackaerts, K., Muys, B., Coppin, P., Weiss, M., & Baret, F. (2004). Review of methods for in situ leaf area index determination: Part I. Theories, sensors and hemispherical photography. *Agricultural and Forest Meteorology*, *121*(1–2), 19–35.

Kalwar, O. P. P., Hussin, Y. A., Weir, M. J. C., & Karna, Y. K. (2016). Derivation of forest inventory parameters for carbon estimation using terrestrial lidar. *ISPRS - International Archives of the Photogrammetry, Remote Sensing and Spatial Information Sciences*, *XLI-B8*, 677–684. https://doi.org/10.5194/isprsarchives-XLI-B8-677-2016

Kissling, W. D., Ahumada, J. A., Bowser, A., Fernandez, M., Fernández, N., García, E. A., Guralnick, R. P., Isaac, N. J. B., Kelling, S., Los, W., McRae, L., Mihoub, J.-B., Obst, M., Santamaria, M., Skidmore, A. K.,

Williams, K. J., Agosti, D., Amariles, D., Arvanitidis, C., … Hardisty, A. R. (2018). Building essential biodiversity variables (EBVs) of species distribution and abundance at a global scale. *Biological Reviews*, *93*(1), 600–625. https://doi.org/10.1111/brv.12359

Kissling, W. D., Shi, Y., Koma, Z., Meijer, C., Ku, O., Nattino, F., Seijmonsbergen, A. C., & Grootes, M. W. (2022). Laserfarm – A high-throughput workflow for generating geospatial data products of ecosystem structure from airborne laser scanning point clouds. *Ecological Informatics*, *72*, 101836. https://doi.org/10.1016/j.ecoinf.2022.101836

Kissling, W. D., Walls, R., Bowser, A., Jones, M. O., Kattge, J., Agosti, D., Amengual, J., Basset, A., van Bodegom, P. M., Cornelissen, J. H. C., Denny, E. G., Deudero, S., Egloff, W., Elmendorf, S. C., Alonso García, E., Jones, K. D., Jones, O. R., Lavorel, S., Lear, D., … Guralnick, R. P. (2018). Towards global data products of Essential Biodiversity Variables on species traits. *Nature Ecology & Evolution*, *2*(10), Article 10. https://doi.org/10.1038/s41559-018-0667-3

Koma, Z., Zlinszky, A., Bekő, L., Burai, P., Seijmonsbergen, A. C., & Kissling, W. D. (2021). Quantifying 3D vegetation structure in wetlands using differently measured airborne laser scanning data. *Ecological Indicators*, *127*, 107752. https://doi.org/10.1016/j.ecolind.2021.107752

Konishi, A., Eguchi, A., Hosoi, F., & Omasa, K. (2009). 3D monitoring spatio–temporal effects of herbicide on a whole plant using combined range and chlorophyll a fluorescence imaging. *Functional Plant Biology*, *36*(11), 874–879.

Kucharik, C. J., Norman, J. M., & Gower, S. T. (1998). Measurements of leaf orientation, light distribution and sunlit leaf area in a boreal aspen forest. *Agricultural and Forest Meteorology*, *91*(1–2), 127–148.

Kumpula Botanic Garden | LUOMUS. (n.d.). Retrieved 28 April 2023, from https://www.luomus.fi/en/kumpula-botanic-garden

Lang, A. (1986). Leaf-Area and Average Leaf Angle From Transmission of Direct Sunlight. *Australian Journal of Botany*, *34*(3), 349. https://doi.org/10.1071/BT9860349

Lang, A. R. G. (1973). Leaf orientation of a cotton plant. *Agricultural Meteorology*, *11*, 37–51. https://doi.org/10.1016/0002-1571(73)90049-6

Lemeur, R., & Blad, B. L. (1974). A critical review of light models for estimating the shortwave radiation regime of plant canopies. *Agricultural Meteorology*, *14*(1), 255–286. https://doi.org/10.1016/0002-1571(74)90024-7

Li, C., Li, H., Li, J., Lei, Y., Li, C., Manevski, K., & Shen, Y. (2019). Using NDVI percentiles to monitor real-time crop growth. *Computers and Electronics in Agriculture*, *162*, 357–363. https://doi.org/10.1016/j.compag.2019.04.026

Li, Y., Guo, Q., & Su, Y. (2018). Retrieving the Leaf area Index of Individual Trees and Stands using Single-Scan Data From a Terrestrial Laser Scanner. *IGARSS 2018 - 2018 IEEE International Geoscience and Remote Sensing Symposium*, 7536–7539. https://doi.org/10.1109/IGARSS.2018.8518911

Li, Y., Su, Y., Hu, T., Xu, G., & Guo, Q. (2018). Retrieving 2-D Leaf Angle Distributions for Deciduous Trees From Terrestrial Laser Scanner Data. *IEEE Transactions on Geoscience and Remote Sensing*, *56*(8), 4945–4955. https://doi.org/10.1109/TGRS.2018.2843382

Liang, X., Hyyppä, J., Kaartinen, H., Lehtomäki, M., Pyörälä, J., Pfeifer, N., Holopainen, M., Brolly, G., Francesco, P., Hackenberg, J., Huang, H., Jo, H.-W., Katoh, M., Liu, L., Mokroš, M., Morel, J., Olofsson, K., Poveda-Lopez, J., Trochta, J., … Wang, Y. (2018). International benchmarking of terrestrial laser scanning approaches for forest inventories. *ISPRS Journal of Photogrammetry and Remote Sensing*, *144*, 137–179. https://doi.org/10.1016/j.isprsjprs.2018.06.021

Liu, G., Wang, J., Dong, P., Chen, Y., & Liu, Z. (2018). Estimating Individual Tree Height and Diameter at Breast Height (DBH) from Terrestrial Laser Scanning (TLS) Data at Plot Level. *Forests*, *9*(7), 398. https://doi.org/10.3390/f9070398

Liu, J., Skidmore, A. K., Wang, T., Zhu, X., Premier, J., Heurich, M., Beudert, B., & Jones, S. (2019). Variation of leaf angle distribution quantified by terrestrial LiDAR in natural European beech forest. *ISPRS Journal of Photogrammetry and Remote Sensing*, *148*, 208–220. https://doi.org/10.1016/j.isprsjprs.2019.01.005

Lugg, D. G., Youngman, V. E., & Hinze, G. (1981). Leaf Azimuthal Orientation of Sorghum in Four Row Directions [1]. *Agronomy Journal*, *73*(3), 497–500. https://doi.org/10.2134/agronj1981.00021962007300030022x

McKnight, P. E., & Najab, J. (2010). Mann-Whitney U Test. In *The Corsini Encyclopedia of Psychology* (pp. 1–1). John Wiley & Sons, Ltd. https://doi.org/10.1002/9780470479216.corpsy0524

McNeil, B. E., Pisek, J., Lepisk, H., & Flamenco, E. A. (2016). Measuring leaf angle distribution in broadleaf canopies using UAVs. *Agricultural and Forest Meteorology*, *218–219*, 204–208. https://doi.org/10.1016/j.agrformet.2015.12.058

Monsi, M. (2004). On the Factor Light in Plant Communities and its Importance for Matter Production. *Annals of Botany*, *95*(3), 549–567. https://doi.org/10.1093/aob/mci052

Monteith, J. L. (1965). Light Distribution and Photosynthesis in Field Crops. *Annals of Botany*, *29*(1), 17–37. https://doi.org/10.1093/oxfordjournals.aob.a083934

Moskal, L. M., & Zheng, G. (2012). Retrieving Forest Inventory Variables with Terrestrial Laser Scanning (TLS) in Urban Heterogeneous Forest. *Remote Sensing*, *4*(1), Article 1. https://doi.org/10.3390/rs4010001

Mu, X., Hu, R., Zeng, Y., McVicar, T. R., Ren, H., Song, W., Wang, Y., Casa, R., Qi, J., & Xie, D. (2017). Estimating structural parameters of agricultural crops from ground-based multi-angular digital images with a fractional model of sun and shade components. *Agricultural and Forest Meteorology*, *246*, 162–177.

Muraoka, H., Takenaka, A., Tang, Y., Koizumi, H., & Washitani, I. (1998). Flexible leaf orientations of Arisaema heterophyllum maximize light capture in a forest understorey and avoid excess irradiance at a deforested site. *Annals of Botany*, *82*(3), 297–307.

Myneni, R. B., Ross, J., & Asrar, G. (1989). A review on the theory of photon transport in leaf canopies. *Agricultural and Forest Meteorology*, *45*(1–2), 1–153.

Niinemets, Ü. (2010). A review of light interception in plant stands from leaf to canopy in different plant functional types and in species with varying shade tolerance. *Ecological Research*, *25*(4), 693–714. https://doi.org/10.1007/s11284-010-0712-4

Niinemets, Ü., & Fleck, S. (2002). Petiole mechanics, leaf inclination, morphology, and investment in support in relation to light availability in the canopy of Liriodendron tulipifera. *Oecologia*, *132*(1), 21–33. https://doi.org/10.1007/s00442-002-0902-z

Nilson, T. (1971). A theoretical analysis of the frequency of gaps in plant stands. *Agricultural Meteorology*, *8*, 25–38. https://doi.org/10.1016/0002-1571(71)90092-6

Norman, J. M., & Campbell, G. S. (1989). Canopy structure. In *Plant physiological ecology* (pp. 301–325). Springer.

Ollinger, S. V. (2011). Sources of variability in canopy reflectance and the convergent properties of plants. *New Phytologist*, *189*(2), 375–394.

Omasa, K., Hosoi, F., & Konishi, A. (2007). 3D lidar imaging for detecting and understanding plant responses and canopy structure. *Journal of Experimental Botany*, *58*(4), 881–898.

Pepe, M., Ackermann, S., Fregonese, L., & Achille, C. (2016). 3D Point cloud model color adjustment by combining terrestrial laser scanner and close range photogrammetry datasets. In *ICDH 2016: 18th International Conference on Digital Heritage* (Vol. 10, pp. 1942-1948). International Journal of Computer and Information Engineering.

Pereira, H. M., Ferrier, S., Walters, M., Geller, G. N., Jongman, R. H. G., Scholes, R. J., Bruford, M. W., Brummitt, N., Butchart, S. H. M., Cardoso, A. C., Coops, N. C., Dulloo, E., Faith, D. P., Freyhof, J., Gregory, R. D., Heip, C., Höft, R., Hurtt, G., Jetz, W., … Wegmann, M. (2013). Essential Biodiversity Variables. *Science*, *339*(6117), 277–278. https://doi.org/10.1126/science.1229931

Pfennigbauer, M., & Ullrich, A. (2010). *Improving quality of laser scanning data acquisition through calibrated amplitude and pulse deviation measurement* (M. D. Turner & G. W. Kamerman, Eds.; p. 76841F). https://doi.org/10.1117/12.849641

Pisek, J., Ryu, Y., & Alikas, K. (2011). Estimating leaf inclination and G-function from leveled digital camera photography in broadleaf canopies. *Trees*, *25*(5), 919–924. https://doi.org/10.1007/s00468-011-0566-6

Point Cloud Library. (n.d.). Point Cloud Library. Retrieved 28 April 2023, from https://pointcloudlibrary.github.io/

Raabe, K., Pisek, J., Sonnentag, O., & Annuk, K. (2015). Variations of leaf inclination angle distribution with height over the growing season and light exposure for eight broadleaf tree species. *Agricultural and Forest Meteorology*, *214–215*, 2–11. https://doi.org/10.1016/j.agrformet.2015.07.008

Ross, J. (1981). *The radiation regime and architecture of plant stands*. Springer Netherlands. https://doi.org/10.1007/978-94-009-8647-3

Royal Botanic Gardens, Kew | Kew. (n.d.). Retrieved 28 April 2023, from https://www.kew.org/

Ryu, Y., Sonnentag, O., Nilson, T., Vargas, R., Kobayashi, H., Wenk, R., & Baldocchi, D. D. (2010). How to quantify tree leaf area index in an open savanna ecosystem: A multi-instrument and multi-model approach. *Agricultural and Forest Meteorology*, *150*(1), 63–76. https://doi.org/10.1016/j.agrformet.2009.08.007

Skidmore, A. K., Coops, N. C., Neinavaz, E., Ali, A., Schaepman, M. E., Paganini, M., Kissling, W. D., Vihervaara, P., Darvishzadeh, R., & Feilhauer, H. (2021). Priority list of biodiversity metrics to observe from space. *Nature Ecology & Evolution*, *5*(7), 896–906.

Stovall, A. E. L., Masters, B., Fatoyinbo, L., & Yang, X. (2021). TLSL e AF: automatic leaf angle estimates from single-scan terrestrial laser scanning. *New Phytologist*, *232*(4), 1876–1892. https://doi.org/10.1111/nph.17548

Stuckens, J., Somers, B., Delalieux, S., Verstraeten, W. W., & Coppin, P. (2009). The impact of common assumptions on canopy radiative transfer simulations: A case study in Citrus orchards. *Journal of Quantitative Spectroscopy and Radiative Transfer*, *110*(1–2), 1–21.

Tadrist, L., Saudreau, M., & de Langre, E. (2014). Wind and gravity mechanical effects on leaf inclination angles. *Journal of Theoretical Biology*, *341*, 9–16.

The Computational Geometry Algorithms Library. (n.d.). Retrieved 28 April 2023, from https://www.cgal.org/index.html

Utsugi, H., Araki, M., Kawasaki, T., & Ishizuka, M. (2006). Vertical distributions of leaf area and inclination angle, and their relationship in a 46-year-old Chamaecyparis obtusa stand. *Forest Ecology and Management*, *225*(1–3), 104–112. https://doi.org/10.1016/j.foreco.2005.12.028

Vicari, M. B. (2017). *tlseparation: Performs the wood/leaf separation from 3D point clouds generated using Terrestrial LiDAR Scanners.* (1.3.3) [Python]. Retrieved 8 May 2023, from https://github.com/TLSeparation/source

Vicari, M. B., Pisek, J., & Disney, M. (2019). New estimates of leaf angle distribution from terrestrial LiDAR: Comparison with measured and modelled estimates from nine broadleaf tree species. *Agricultural and Forest Meteorology*, *264*, 322–333. https://doi.org/10.1016/j.agrformet.2018.10.021

Wagner, S., & Hagemeier, M. (2006). Method of segmentation affects leaf inclination angle estimation in hemispherical photography. *Agricultural and Forest Meteorology*, *139*(1–2), 12–24.

Wang, W.-M., Li, Z.-L., & Su, H.-B. (2007). Comparison of leaf angle distribution functions: Effects on extinction coefficient and fraction of sunlit foliage. *Agricultural and Forest Meteorology*, *143*(1–2), 106–122. https://doi.org/10.1016/j.agrformet.2006.12.003

Weber, J., & Penn, J. (1995). Creation and rendering of realistic trees. *Proceedings of the 22nd Annual Conference on Computer Graphics and Interactive Techniques*, 119–128.

Weiss, M., Baret, F., Smith, G. J., Jonckheere, I., & Coppin, P. (2004). Review of methods for in situ leaf area index (LAI) determination: Part II. Estimation of LAI, errors and sampling. *Agricultural and Forest Meteorology*, *121*(1), 37–53. https://doi.org/10.1016/j.agrformet.2003.08.001

Wezyk, P., Koziol, K., Glista, M., & Pierzchalski, M. (2007). Terrestrial laser scanning versus traditional forest inventory first results from the polish forests. *ISPRS Workshop on Laser Scanning*, 12–14.

Widlowski, J.-L., Mio, C., Disney, M., Adams, J., Andredakis, I., Atzberger, C., Brennan, J., Busetto, L., Chelle, M., Ceccherini, G., Colombo, R., Côté, J.-F., Eenmäe, A., Essery, R., Gastellu-Etchegorry, J.-P., Gobron, N., Grau, E., Haverd, V., Homolová, L., … Zenone, T. (2015). The fourth phase of the radiative transfer model intercomparison (RAMI) exercise: Actual canopy scenarios and conformity testing. *Remote Sensing of Environment*, *169*, 418–437. https://doi.org/10.1016/j.rse.2015.08.016

Wilson, J. W. (1960). Inclined Point Quadrats. *New Phytologist*, *59*(1), 1–7. https://doi.org/10.1111/j.1469-8137.1960.tb06195.x

Wilson, J. W. (1967). Stand Structure and Light Penetration. III. Sunlit Foliage Area. *Journal of Applied Ecology*, *4*(1), 159–165. https://doi.org/10.2307/2401415

Wit, C. T. de. (1965). *Photosynthesis of leaf canopies* (No. 663; p.). Pudoc. https://library.wur.nl/WebQuery/wurpubs/413358

Xiao, Q., McPherson, E. G., Ustin, S. L., & Grismer, M. E. (2000). A new approach to modeling tree rainfall interception. *Journal of Geophysical Research: Atmospheres*, *105*(D23), 29173–29188.

Xu, Q., Cao, L., Xue, L., Chen, B., An, F., & Yun, T. (2018). Extraction of Leaf Biophysical Attributes Based on a Computer Graphic-based Algorithm Using Terrestrial Laser Scanning Data. *Remote Sensing*, *11*(1), 15. https://doi.org/10.3390/rs11010015

Yan, G., Hu, R., Luo, J., Weiss, M., Jiang, H., Mu, X., Xie, D., & Zhang, W. (2019). Review of indirect optical measurements of leaf area index: Recent advances, challenges, and perspectives. *Agricultural and Forest Meteorology*, *265*, 390–411.

Yang, X., Strahler, A. H., Schaaf, C. B., Jupp, D. L. B., Yao, T., Zhao, F., Wang, Z., Culvenor, D. S., Newnham, G. J., Lovell, J. L., Dubayah, R. O., Woodcock, C. E., & Ni-Meister, W. (2013). Three-dimensional forest reconstruction and structural parameter retrievals using a terrestrial full-waveform lidar instrument (Echidna®). *Remote Sensing of Environment*, *135*, 36–51. https://doi.org/10.1016/j.rse.2013.03.020

Zhao, F., Yang, X., Schull, M. A., Román-Colón, M. O., Yao, T., Wang, Z., Zhang, Q., Jupp, D. L., Lovell, J. L., & Culvenor, D. S. (2011). Measuring effective leaf area index, foliage profile, and stand height in New England forest stands using a full-waveform ground-based lidar. *Remote Sensing of Environment*, *115*(11), 2954–2964.

Zhao, K., García, M., Liu, S., Guo, Q., Chen, G., Zhang, X., Zhou, Y., & Meng, X. (2015). Terrestrial lidar remote sensing of forests: Maximum likelihood estimates of canopy profile, leaf area index, and leaf angle distribution. *Agricultural and Forest Meteorology*, *209–210*, 100–113. https://doi.org/10.1016/j.agrformet.2015.03.008

Zhao, K., Ryu, Y., Hu, T., Garcia, M., Li, Y., Liu, Z., Londo, A., & Wang, C. (2019). How to better estimate leaf area index and leaf angle distribution from digital hemispherical photography? Switching to a binary nonlinear regression paradigm. *Methods in Ecology and Evolution*, *10*(11), 1864–1874.

Zheng, G., & Moskal, L. M. (2009). Retrieving leaf area index (LAI) using remote sensing: Theories, methods and sensors. *Sensors*, *9*(4), 2719–2745.

Zheng, G., & Moskal, L. M. (2012). Leaf Orientation Retrieval from Terrestrial Laser Scanning (TLS) Data. *IEEE Transactions on Geoscience and Remote Sensing*, *50*(10), 3970–3979. https://doi.org/10.1109/TGRS.2012.2188533

Zheng, G., Moskal, L. M., & Kim, S.-H. (2013). Retrieval of Effective Leaf Area Index in Heterogeneous Forests With Terrestrial Laser Scanning. *IEEE Transactions on Geoscience and Remote Sensing*, *51*(2), 777–786. https://doi.org/10.1109/TGRS.2012.2205003

Zou, X., Mõttus, M., Tammeorg, P., Torres, C. L., Takala, T., Pisek, J., Mäkelä, P., Stoddard, F. L., & Pellikka, P. (2014). Photographic measurement of leaf angles in field crops. *Agricultural and Forest Meteorology*, *184*, 137–146. https://doi.org/10.1016/j.agrformet.2013.09.010